HHS Public Access

Author manuscript

Cell Metab. Author manuscript; available in PMC 2024 February 07.

Published in final edited form as:

Cell Metab. 2023 February 07; 35(2): 316–331.e6. doi:10.1016/j.cmet.2022.12.005.

Metabolic adaptation supports enhanced macrophage efferocytosis in limited-oxygen environments

Ya-Ting Wang[1], **Alissa J. Trzeciak**[1], **Waleska Saitz Rojas**[1], **Pedro Saavedra**[1], **Yan-Ting Chen**[2], **Rachel Chirayil**[3,4], **Jon Iker Etchegaray**[5], **Christopher D. Lucas**[6,7], **Daniel J. Puleston**[8], **Kayvan R. Keshari**[3,4], **Justin S. A. Perry**[1,2,9,^]

[1]Immunology Program, Memorial Sloan Kettering Cancer Center, New York, NY, United States.

[2]Louis V. Gerstner Jr. Graduate School of Biomedical Sciences, Memorial Sloan Kettering Cancer Center, New York, NY, USA.

[3]Department of Radiology, Memorial Sloan Kettering Cancer Center, New York, NY, USA.

[4]Molecular Pharmacology Program, Memorial Sloan Kettering Cancer Center, New York, NY, USA.

[5]Department of Microbiology, Immunology, and Cancer Biology, University of Virginia, Charlottesville, VA, USA.

[6]University of Edinburgh Centre for Inflammation Research, Queen's Medical Research Institute, Edinburgh BioQuarter, UK.

[7]Institute for Regeneration and Repair, Edinburgh BioQuarter, UK.

[8]Bloomberg-Kimmel Institute of Cancer Immunotherapy, Sidney Kimmel Comprehensive Cancer Center, Johns Hopkins University, Baltimore, MD, USA.

[9]Department of Immunology and Microbial Pathogenesis, Weill Cornell Medical College, New York, NY, USA.

Summary

Apoptotic cell (AC) clearance (efferocytosis) is performed by phagocytes, such as macrophages, that inhabit harsh physiological environments. Here, we find macrophages display enhanced efferocytosis under prolonged (chronic) physiological hypoxia, characterized by increased internalization and accelerated degradation of ACs. Transcriptional and translational analysis

^Corresponding author: perryj@mskcc.org.

Author Contributions

Y.-T.W. and J.S.A.P. planned and executed the majority of the experiments. W.S.R., A.T., P.S., and Y.-T.C. assisted with the performance and analysis of key *in vitro*/*in vivo* experiments. R.C. and K.R.K. planned and executed NMR experiments. J.I.E, C.D.L., and D.J.P. assisted with the analysis and interpretation of *in vivo*/*ex vivo* experiments. All authors assisted in the preparation and review of the manuscript.

Declaration of Interests

K.R.K. Serves on the scientific advisory board of NVision Imaging Technologies. J.S.A.P. and K.R.K holds patents related to imaging and modulation of cellular metabolism.

revealed that chronic physiological hypoxia induces two distinct but complimentary states. The first, ‘primed’ state consists of concomitant transcription and translation of metabolic programs in AC-naïve macrophages that persist during efferocytosis. The second, ‘poised’ state consists of transcription, but not translation, of phagocyte function programs in AC-naïve macrophages that are translated during efferocytosis. Mechanistically, macrophages efficiently flux glucose into a noncanonical pentose phosphate pathway (PPP) loop to enhance NADPH production. PPP-derived NADPH directly supports enhanced efferocytosis under physiological hypoxia by ensuring phagolysosomal maturation and redox homeostasis. Thus, macrophages residing under physiological hypoxia adopt states that support cell fitness and ensure performance of essential homeostatic functions rapidly and safely.

eTOC

Tissues pose distinct challenges that macrophages must overcome, including limited nutrient availability (glucose, oxygen), to perform essential functions such as apoptotic cell clearance (efferocytosis). Here, Wang et al. find that macrophages undergo novel metabolic adaptations to prolonged physiological hypoxia that directly support rapid, efficient efferocytosis.

Graphical Abstract

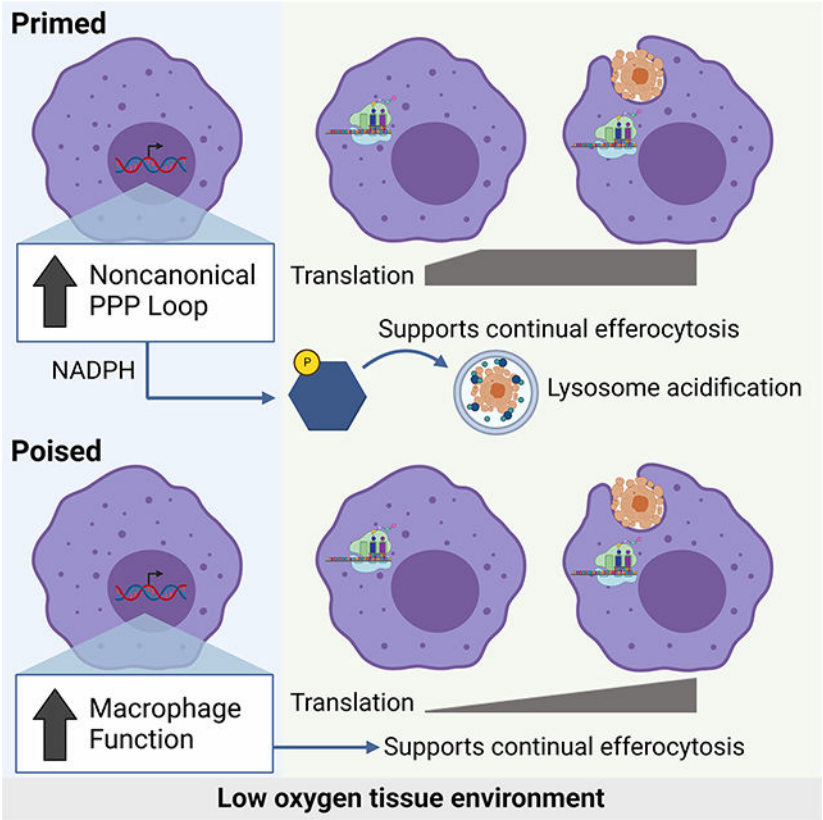

Introduction

Efferocytosis, the phagocytic clearance of apoptotic cells (ACs), is indispensable for organismal homeostasis[1–3]. Efferocytosis occurs in all major tissues and organs, ensuring that disparate processes such as barrier epithelial cell recycling, removal of spent neutrophils and red blood cells, elimination of apoptotic neurons, and clearance of negatively-selected thymocytes are executed rapidly and safely[4–6]. These clearance processes are performed by various types of phagocytes, especially by tissue-resident macrophages (TRMs[7,8]). At homeostasis, each tissue exhibits a substantial rate of cellular turnover, collectively amounting to ~1–2% body mass each day[9]. As the body's main professional phagocyte, TRMs shoulder the brunt of this massive burden[10].

TRMs are generally long-lived cells that seed a tissue early during development and often reside in a tissue throughout the organism's lifespan[11–14]. It is now clear that TRMs adapt to their unique and often harsh tissue environment to perform their core functions[11,13,15], including residing in tissues with a relative dearth of oxygen availability and exposure to tissue-specific debris and metabolites. For instance, the tissues that feature the most cell turnover (bone marrow, spleen, thymus[9,16,17] are also tissues with the lowest oxygen availability (~1% O_2, termed physiological hypoxia[18–20]). TRMs, then, must both adapt to the tissue environment in which they reside and cope with the continuous influx of internalized biological material. Recent work has illustrated mechanisms by which phagocytes sense and respond to internalized ACs[21–25], however, how tissue environment factors, such as oxygen availability, inform the ability to perform efferocytosis remains unknown.

Here, we made the striking discovery that exposure to prolonged ('chronic') physiological hypoxia, similar to that experienced by several TRM populations, resulted in increased internalization and accelerated degradation of ACs. We found that chronic exposure to physiological hypoxia induced two distinct but complimentary states. One state, which we term 'primed', generally consists of simultaneous transcriptional and translational induction or suppression of metabolic programs in AC-naïve macrophages that remain induced or suppressed during efferocytosis. The other state, which we term 'poised', generally consists of transcription, without concomitant translation, of phagocytic functional programs in AC-naïve macrophages that are instead translated during efferocytosis. Importantly, we discovered that both states are necessary for enhanced continual efferocytosis. Subsequent exploration of primed state metabolic programs revealed that macrophages exposed to chronic physiological hypoxia switch to the efficient utilization of glucose to generate NADPH via a noncanonical pentose phosphate pathway (PPP) loop that features recycling of PPP-derived intermediates back through the oxidative PPP. The PPP-dependent generation of NADPH prior to efferocytosis served to both support enhanced internalization and degradation of ACs via phagolysosomal maturation and protect phagocytes from runaway oxidative stress. These studies reveal that local tissue environment, in this case physiological hypoxia, programs distinct states in macrophages that simultaneously support cell fitness and ensure the ability to perform critical homeostatic functions, such as efferocytosis.

Results

Efferocytosis is enhanced under prolonged ('chronic') physiological hypoxia

To address the effect of prolonged ('chronic') physiological hypoxia on efferocytosis, we optimized a system and protocols to continually manipulate and culture primary professional phagocytes (macrophages) in low (1%) oxygen. Strikingly, chronic physiological hypoxia-conditioned macrophages internalized significantly more ACs than both macrophages cultured under atmospheric ('standard') oxygen levels (21%) and macrophages exposed to 'acute' (3h) hypoxia (Figure 1A). Chronic physiological hypoxia-conditioned macrophages internalized significantly more ACs irrespective of the size of the target cell, the type of target cell, the method of cell death induction, or the transformation status of the target cell (Figure 1B; Figure S1A–D). Furthermore, macrophages internalized significantly more ACs regardless of whether they were initially differentiated in standard oxygen or under physiological hypoxia prior to conditioning (Figure 1C), and this enhanced efferocytosis capacity was lost in chronic physiological hypoxia-conditioned macrophages when transferred back to standard oxygen conditions (Figure S1E).

Professional phagocytes are often responsible for internalization of ACs in quick succession, a phenomenon known as 'continual efferocytosis', which protects against the manifestation of inflammatory disease, such as atherosclerosis[23,24,26,27]. Interestingly, chronic physiological hypoxia-conditioned macrophages also exhibited significantly higher levels of continual efferocytosis (Figure 1D). Despite the increased proportion of macrophages internalize more ACs on a population level, our flow cytometric analysis of the geometric mean fluorescence intensity of AC uptake (a surrogate of per-cell uptake) was similar between conditions (Figure S1F), suggesting that either 1) individual macrophages do not take up more ACs, or 2) chronic physiological hypoxia-conditioned macrophages internalize more ACs and digest internalized ACs quicker on a per-cell basis. To test these hypotheses, we performed time-lapse confocal microscopy of macrophages conditioned in standard oxygen or chronic physiological hypoxia. Indeed, chronic physiological hypoxia-conditioned macrophages not only internalized significantly more ACs on a per-cell basis but also degraded internalized ACs significantly faster (Figure 1E and 1F).

Multiple tissue-resident macrophage populations reside under physiological hypoxia. For instance, bone marrow-resident macrophages and macrophage subsets in the spleen chronically experience oxygen levels as low as ~1%[19]. To test the *in vivo* relevance of physiological hypoxia on efferocytosis, we isolated tissue-resident macrophages (TRMs) from either the bone marrow or spleen and seeded them in either standard or 1% oxygen (Figure 1G and 1H). Consistent with our *in vitro* conditioning studies, we found that both bone marrow and splenic TRMs exhibited higher efferocytosis when maintained in 1% oxygen compared to standard oxygen (Figure 1G and 1H). Collectively, our data suggest that professional phagocytes better internalize and degrade potentially dangerous ACs under prolonged physiological hypoxia.

Characterization of macrophages under chronic physiological hypoxia

To investigate how macrophages adapt to chronic physiological hypoxia, we performed RNA sequencing (RNAseq) of primary macrophages cultured in standard oxygen (21%), exposed to acute hypoxia (1% for 3h), and exposed to prolonged physiological hypoxia (1% for 7d; Figure 2A). Analysis of chronic physiological hypoxia-conditioned macrophages revealed several differentially expressed transcriptional programs (Figure 2B). For instance, we observed significant downregulation of lipid and mitochondrial metabolism programs and upregulation of carbohydrate metabolism and hypoxia-responsive programs (Figure 2B), broadly consistent with a previous study of cancerous cells cultured under chronic hypoxia[28]. We observed several programs not previously associated with physiological hypoxia. For instance, we observed downregulation of metabolic programs (e.g., amino acid metabolism, insulin signaling), cell biological processes (e.g., endocytosis, vesicular transport), and immunity (e.g., pro-inflammatory, antigen presentation) (Figure 2B; Figure S2A and S2B). Contrarily, we observed upregulation of homeostatic macrophage function programs (e.g., phagocytosis, wound healing), cell biological processes (e.g., lysosome biology, cell adhesion), and pro-tumorigenic programs (Figure 2B; Figure S2A and S2B). Although the majority of the chronic physiological hypoxia-specific program was induced only after prolonged hypoxia, a fraction of the program was modestly, albeit non-significantly, induced in response to acute hypoxia (Chronic vs. Standard Only; Figure 2C). Because these genes significantly increase after prolonged physiological hypoxia, we consider them part of the chronic physiological hypoxia-induced program.

In parallel, we performed proteomic analysis of chronic physiological hypoxia-conditioned macrophages. Our analysis revealed several differentially regulated programs that overlap with programs identified via RNAseq, especially programs involved in cellular metabolism (Figure 2D). We validated representative targets fitting into one of three criteria: 1) a target upregulated in both RNAseq and proteomics analysis, Arginase 1 (ARG1, gene symbol *Arg1*), 2) a target downregulated in both RNAseq and proteomics analysis, transferrin receptor protein 1 (CD71, gene symbol *Tfrc*), and 3) a target upregulated in RNAseq but not detected via proteomics, 4–1BB (CD137, gene symbol *Tnfrs9*) (Figure 2E). Taken together, these data indicate that macrophages induce unique gene and protein programs in response to chronic physiological hypoxia.

Chronic physiological hypoxia induces states both primed and poised for efferocytosis

Beyond differentially-regulated genes that we failed to detect signal for in our proteomics analysis, we also observed that a plurality of genes differentially regulated under chronic hypoxia are detected but remain unchanged at the protein level (Figure S3A). One hypothesis is that macrophages in low oxygen environments accumulate function-specific mRNAs that allow for rapid protein synthesis during the execution of canonical functions. To test this, we used a strategy for performing mass spectrometry analysis of proteins in efferocytotic macrophages while excluding contaminating peptides from internalized ACs. Specifically, we labeled live target cells with ^{13}C-lysine prior to use in efferocytosis assay (Figure 3A and Figure S3B). Analysis of the core chronic physiological hypoxia-induced mRNA program revealed two distinct patterns of protein expression. First, we observed transcriptional programs that were also significantly differentially expressed

at the protein level in AC-naïve macrophages, which remained differentially expressed in efferocytotic macrophages ('Primed' Programs, Figure 3A; Figure S4, PFKL/*Pfkl* in Figure 3B). This cluster consisted primarily of cellular metabolism programs. Second, we observed programs differentially regulated at the mRNA level but not the protein level in AC-naïve macrophages, that were subsequently differentially regulated at the protein level in efferocytotic macrophages ('Poised' Programs, Figure 3A; Figure S4, SAMD9L/*Samd9l* in Figure 3B). This cluster consisted primarily of macrophage function programs, including phagocytosis. Thus, chronic physiological hypoxia induces two distinct but complementary states in macrophages. The first 'primed' state responds immediately by coupling transcription and translation to prime AC-naïve macrophages for efferocytosis. The second 'poised' state features transcriptional changes without concomitant translation in AC-naïve macrophages, instead poising AC-naïve macrophages with function-specific transcripts that are subsequently translated during efferocytosis.

Our discovery of 'poised' state programs raised the question, what purpose does enhanced transcription of core functional genes without concomitant protein synthesis serve? One hypothesis is that translation of 'poised' state programs is necessary to support continuous uptake and degradation of ACs observed in chronic physiological hypoxia-conditioned macrophages. To test this, we took advantage of the properties of cycloheximide (Chx) to temporally-disrupt translation with minimal effect on transcription (Figure 3C). Treatment of standard oxygen-conditioned macrophages with Chx immediately prior to culture with ACs did not affect efferocytosis (Figure 3C). Contrarily, treatment of chronic physiological hypoxia-conditioned macrophages with Chx immediately prior to culture with ACs resulted in a significant decrease in efferocytosis (Figure 3C). Furthermore, we tested if disrupting translation affects per-cell internalization and AC degradation rate. We observed that chronic physiological hypoxia-conditioned macrophages treated with Chx internalized significantly fewer ACs on a per-cell basis (Figure 3D, top graph). Additionally, temporally disrupted translation resulted in a slower rate of AC degradation (Figure 3D, bottom graph), suggesting that translation of the 'poised' program is essential for rapid, continuous efferocytosis observed in chronic physiological hypoxia-conditioned macrophages.

Finally, we sought to determine if the 'poised' program is important for efferocytosis *in vivo*. Many of the tissues where macrophages perform high efferocytosis burden feature physiological hypoxia[8]. For instance, macrophages in the thymus are responsible for clearing millions of apoptotic thymocytes daily[16,17] despite the thymus featuring physiological hypoxia (10mmHg, or ~1%, O_2[29]). Taking advantage of its *in vivo* activity, we treated mice with Chx or vehicle prior to the induction of thymocyte apoptosis using dexamethasone (Figure 3E). Similar to our *in vitro* findings, mice treated with Chx exhibited significantly decreased clearance of apoptotic thymocytes (Figure 3E). Thus, the 'poised' program observed in chronic physiological hypoxia-conditioned macrophages is necessary for efficient continual efferocytosis *in vitro* and *in vivo*.

Mapping the metabolic pathways unique to chronic hypoxia-conditioned macrophages

We further explored macrophage metabolism under chronic physiological hypoxia. We first performed a network analysis of the differentially regulated metabolic programs in

'primed' macrophages (Figure 4A, Figure S4A). Our analysis revealed that the broader metabolic programs clustered into specific metabolic pathways. For instance, carbohydrate metabolism clustered into three categories: gluconeogenesis/ glucose transport, one carbon/ aldehyde metabolism, and pentose phosphate pathway (PPP; Figure 4A). Consistent with our RNAseq and proteomics analyses, we observed significant differences in glucose uptake by macrophages conditioned in hypoxia (Figure 4B). However, contrary to our expectations, we observed that chronic physiological hypoxia-conditioned macrophages consume significantly less glucose from media than macrophages in standard oxygen (Figure 4B, left graph). Furthermore, chronic physiological hypoxia-conditioned macrophages secrete less lactate (Figure 4B, right graph) and contain less ATP (Figure 4C).

Our findings that chronic physiological hypoxia-conditioned macrophages consume and utilize less glucose was surprising given previous studies[30–32]. To further elucidate the metabolic state of chronic physiological hypoxia-conditioned macrophages, we performed untargeted metabolomics analysis. Chronic physiological hypoxia-conditioned macrophages exhibited a different metabolite profile than macrophages from either standard or acute hypoxia conditions (Figure S4B). Our analysis revealed significant upregulation of PPP, polyamine, and vitamin B6 metabolism (Figure 4D and 4E; Figure S4C). On the other hand, we observed downregulation of alanine/aspartate/glutamine, glycine/serine (one carbon), and niacin/nicotinamide (vitamin B3) metabolism (Figure 4D and 4E; Figure S4C). We also observed decreased TCA cycle intermediates (Figure S4C), consistent with our observation that chronic physiological hypoxia-conditioned macrophages downregulate mitochondrial metabolism transcriptionally (Figure S4A). Analysis of individual metabolites revealed relative enrichment of key PPP and upper glycolysis intermediates but downregulated/ unchanged downstream glycolysis intermediates (Figure 4D; Figure S4C). Thus, chronic physiological hypoxia-conditioned macrophages induce or suppress distinct metabolic programs, including increased PPP activity, despite decreased glucose uptake/lactate secretion and ATP synthesis.

Macrophages adapt to chronic physiological hypoxia by co-opting a noncanonical pentose phosphate loop to ensure redox homeostasis

Beyond ATP generated via glycolysis, glucose also contributes to redox homeostasis and nucleotide synthesis by shunting the intermediate glucose 6-phosphate (G6P) into the PPP (Figure 5A). Our finding that chronic physiological hypoxia-conditioned macrophages consume less glucose, secrete less lactate, contain less ATP, and accumulate fewer TCA cycle intermediates but accumulate PPP intermediates suggests that macrophages are using glucose in an unconventional way. One possibility is that chronic physiological hypoxia-conditioned macrophages accumulate PPP intermediates because of efficient shunting of glucose into the PPP. To test this hypothesis, we performed 1,2-^{13}C-glucose tracing of standard oxygen- and chronic physiological hypoxia-conditioned macrophages, which allows us to track intermediates stemming from glucose uptake (Figure 5A[33]). In chronic physiological hypoxia-conditioned macrophages, we observed increased fractional enrichment and relative abundance of several intermediates that had cycled through the PPP (Figure 5A; Figure S5A). Contrarily, we observed decreased fractional enrichment and relative abundance of the terminal glycolysis intermediates phosphoenolpyruvate (PEP) and

lactate as well as decreased contribution of glucose to the glucose-alanine and TCA cycles in chronic physiological hypoxia-conditioned macrophages (Figure S5A). Importantly, we detected significantly less M+1 and M+2 lactate in conditioned media from chronic physiological hypoxia-conditioned macrophages using carbon nuclear magnetic resonance (Figure 5B), suggesting that chronic physiological hypoxia-conditioned macrophages utilize less glucose for energy generation via glycolysis, instead efficiently shunting glucose into the PPP.

As part of our 1,2-^{13}C-glucose tracing studies, we observed intermediates with ^{13}C labeling beyond the first and second position (Figure 5C; Figure S5B). For instance, we observed increased fractional enrichment and relative abundance of M+3, M+4, and M+5 isotopologues of G6P in chronic physiological hypoxia-conditioned macrophages (Figure 5C; Figure S5B). The presence of these isotopologues could only arise if intermediates generated during glycolysis or PPP cycled back to G6P, through a process resembling gluconeogenesis in the liver. Unlike conventional gluconeogenesis, however, we did not detect newly synthesized glucose. Instead, together with G6P, we observe increased fractional enrichment and relative abundance of newly synthesized glycolytic intermediates (Figure 5C). Additionally, we observed increased relative abundance and fractional enrichment of newly synthesized isotopologues of S7P (Figure 5C; Figure S5B). In parallel, we performed uniformly-labeled (U)-^{13}C-glucose tracing of standard oxygen- and chronic physiological hypoxia-conditioned macrophages to directly test glucose carbon recycling and turnover (Figure 5D). Similar to our 1,2-^{13}C-glucose tracing studies, we observed less fractional enrichment and relative abundance of the glycolysis-generated M+3 lactate isotopologue in chronic physiological hypoxia conditioned macrophages (Figure 5D; Figure S5C). Furthermore, chronic physiological hypoxia-conditioned macrophages exhibited increased fractional enrichment and relative abundance of newly-synthesized M+3 G6P and F6P isotopologues (Figure 5D; Figure S5C). Chronic physiological hypoxia-conditioned macrophages also produced less alanine and decreased contribution to the TCA cycle, irrespective of route (via M+2 citrate or M+3 oxaloacetate, Figure S5D and S5E). Finally, glucose that enters the PPP can provide the five-carbon nucleoside sugar necessary for *de novo* nucleotide synthesis. We observed decreased *de novo* synthesis of both inosine monophosphate (IMP) and guanosine monophosphate (GMP; Figure S6F) in chronic physiological hypoxia-conditioned macrophages, suggesting that the adaptation macrophages undergo in response to physiological hypoxia includes a specific and efficient repurposing of glucose for the generation of NADPH.

Although the conventional PPP is important for inflammatory macrophage function, this often coincides with enhanced glycolysis, decreased G6P, and increased TCA cycle intermediates[34–36]. Contrarily, we observe increased PPP absent the other features present in inflammatory macrophages, suggesting that chronic physiological hypoxia-conditioned macrophages co-opt an unconventional PPP. In support of this, we detected M+0 and M+2 sedoheptulose 1,7-bisphosphate (SBP) only in chronic physiological hypoxia-conditioned macrophages (Figure 5C). SBP is an unusual metabolite, previously identified as a novel PPP intermediate in the liver (L-type PPP[37–39]). Interestingly, a recent report found that SBP accumulates in the hepatoma HepG2 line in response to oxidative stress[37], suggesting that cells upregulate the noncanonical PPP to cope with contexts that pose a danger to redox

homeostasis. Indeed, chronic physiological hypoxia-conditioned macrophages exhibited increased synthesis of NADPH and a decreased NADP+/NADPH ratio (Figure 5E, Figure S7A). Furthermore, macrophages exhibit lower cellular oxidative stress (Figure 5F) and lipid peroxidation (Figure 5G), further supporting the notion that macrophages adapt to physiological hypoxia by efficiently enhancing reductive potential and actively maintaining redox homeostasis.

Our RNAseq and proteomic analyses suggested that macrophages respond to chronic physiological hypoxia by regulating mitochondrial metabolism and biology programs (Figure 2 and 3A; Figure S2, S3C, and S5A), which are major regulators of redox state[40]. Subsequent analysis of chronic physiological hypoxia-conditioned macrophages revealed decreased mitochondrial mass and potential (Figure S7B and S7C) and decreased mitochondrial superoxide levels (Figure S6D), suggesting that macrophages limit mitochondrial processes that produce reactive species when exposed to prolonged physiological hypoxia. Additionally, we observed an increased ratio of reduced glutathione (GSH) to oxidized glutathione (GSSG) (Figure 5H) despite decreased glutathione synthesis (Figure S7E) in chronic physiological hypoxia-conditioned macrophages relative to standard oxygen-conditioned macrophages. Collectively, our data indicate that macrophages adapt to chronic physiological hypoxia by preferentially shunting glucose into a noncanonical PPP loop that enhances reductive potential, including increased NADPH generation, to maintain low levels of cellular oxidative stress.

The noncanonical pentose phosphate pathway loop supports continual efferocytosis

We hypothesized that induction of ‘primed’ programs in macrophages exposed to prolonged physiological hypoxia directly support ‘poised’ functional programs, such as efferocytosis. We tested whether induction of noncanonical PPP activity, one of the chronic physiological hypoxia-induced ‘primed’ programs, directly supports efferocytosis. Specifically, we used multiple strategies to target the PPP specifically during efferocytosis (Figure S7F). First, use of the noncompetitive inhibitor of glucose-6-phosphate dehydrogenase (G6PD), G6PDi1, resulted in decreased efferocytosis by chronic physiological hypoxia-conditioned macrophages but not macrophages cultured in standard oxygen (Figure S7G, left graph). Second, treatment with the small molecule inhibitor 6-aminonicotinamide (6-AN), to target G6PD activity, also resulted in significantly decreased efferocytosis in chronic physiological hypoxia-conditioned macrophages (Figure S7G, center graph). Third, to test the contribution of conversion of fructose 1,6-bisphosphate to fructose 6-phosphate, we targeted fructose 1,6-bisphosphatase-1 (FBP1) activity using the selective inhibitor FBPi. Consistent with our tracing studies suggesting that PPP intermediates cycle back to G6P, we found that FBP1 inhibition led to decreased efferocytosis exclusively in chronic physiological hypoxia-conditioned macrophages (Figure S7G, right graph). Collectively, our combination of approaches temporally targeting components of the noncanonical PPP loop suggest that macrophages depend on this loop for efficient efferocytosis under prolonged physiological hypoxia.

We next queried whether PPP activity supports continual efferocytosis. Temporal targeting of G6PD activity not only suppressed internalization of the first AC but also reduced

internalization of subsequent ACs (Figure 6A). Continual efferocytosis depends on a phagocytes ability to rapidly mature the phagolysosome and degrade ACs, as observed in chronic physiological hypoxia-conditioned macrophages (Figure 1E and 1F). Indeed, time-lapse confocal microscopy revealed three key findings. First, inhibition of G6PD activity resulted in fewer macrophages internalizing ACs (Figure 6B). Second, macrophages internalize significantly fewer ACs on a per-cell basis when G6PD activity was inhibited (Figure 6B, top graph). Third, inhibition of G6PD activity resulted in a slower rate of AC degradation (Figure 6B, bottom graph), essentially reversing the 'primed' adaptations macrophages undergo during prolonged physiological hypoxia. Finally, we sought to determine if temporal perturbation of the 'primed' program affects efferocytosis *in vivo*. We treated mice with 6-AN or vehicle prior to the induction of thymocyte apoptosis using dexamethasone (Figure 6C). Similar to our *in vitro* findings and two recent independent studies[41,42], mice treated with 6-AN exhibited significantly decreased clearance of apoptotic thymocytes (Figure 6C).

We next sought to determine if genetic targeting of *G6pdx*, the mouse isoform of G6PD, affects efferocytosis by chronic physiological hypoxia-conditioned macrophages. Similar to our results with the small molecule 6-AN, targeting of *G6pdx* (Figure S7H) revealed several striking findings. First, macrophages lacking *G6pdx* internalized significantly fewer ACs on a per-cell basis (Figure 6D, top graph). Second, macrophages lacking *G6pdx* degraded ACs at a slower rate (Figure 6D, bottom graph), essentially reversing the 'primed' adaptations macrophages make under prolonged physiological hypoxia. This decreased efferocytosis capacity was due to G6PDX deficiency directly, as introduction of a *G6pdx* ORF significantly rescued efferocytosis capacity (Figure S7I). Finally, *G6pdx*-deficient macrophages internalized significantly fewer ACs than control macrophages *in vivo* (Figure 6E). Thus, the 'primed' program, in particular the noncanonical PPP loop, is necessary for efficient continual efferocytosis *in vitro* and *in vivo*.

Noncanonical pentose phosphate loop supports phagolysosomal maturation and prevents redox crisis in efferocytotic macrophages

Phagolysosomal maturation and subsequent AC degradation requires NADPH oxidase activity[43] but if not buffered against, can lead to redox crisis featuring runaway lysosomal acidification and oxidative stress[44,45]. Macrophages under standard oxygen produce minimal NADPH (Figure 7A[45]). On the other hand, we observed significant PPP-dependent production of NADPH (Figure 7A). Although NADPH production remained abundant during efferocytosis by chronic physiological hypoxia-conditioned macrophages (Figure 7B), NADPH pools were further depleted in efferocytotic macrophages with temporally disrupted PPP activity (Figure 7B) and decreased *G6pdx* levels (Figure 7C). Thus, chronic physiological hypoxia-conditioned macrophages boost PPP-dependent NADPH production prior to efferocytosis which remains active during efferocytosis.

Our observation that chronic physiological hypoxia-conditioned macrophages increase PPP-dependent NADPH production both prior to and during efferocytosis raises the hypothesis that the noncanonical PPP loop, a core 'primed' program, directly supports efferocytosis, a core 'poised' program. To test this hypothesis, we sought to determine if

temporal perturbation or genetic disruption of the PPP also leads to runaway lysosomal acidification and oxidative stress in efferocytotic macrophages. In AC-naïve macrophages, inhibition of PPP activity resulted in a modest increase in lysosomal acidity (Figure 7D; Figure S7J). On the other hand, efferocytotic macrophages with perturbed PPP activity displayed significantly higher lysosomal acidity than untreated AC-naïve and efferocytotic macrophages (Figure 7D; Figure S7J). We observed similar results in chronic physiological hypoxia-conditioned macrophages with genetic disruption of *G6pdx* (Figure 7E). Finally, we tested the hypothesis that disrupted PPP activity leads to increased oxidative stress in efferocytotic macrophages. Indeed, we observed that temporal perturbation of PPP activity resulted in significantly increased lipid peroxidation (Figure S7K) and cellular oxidative stress (Figure 7F; Figure S7L) in chronic physiological hypoxia-conditioned efferocytotic macrophages. Importantly, genetic disruption of *G6pdx* also resulted in higher oxidative stress in chronic physiological hypoxia-conditioned efferocytotic macrophages (Figure 7G). Thus, our data suggest that PPP-mediated NADPH production, a core 'primed' program, supports enhanced efferocytosis, a core 'poised' program, by providing the NADPH necessary for both rapid phagolysosomal maturation and protection from excessive lysosomal acidification and oxidative stress under settings of prolonged physiological hypoxia.

Discussion

Professional phagocytes, such as macrophages, reside in tissues throughout the body in limited nutrient environments often for long periods of time[13,15]. This is especially true for oxygen, which ranges between 38 mmHg (~5%) and 10 mmHg (~1%, physiological hypoxia[18]). Despite the relative dearth of oxygen, phagocytes remain responsible for removing millions of ACs daily[19], a process that is metabolically demanding and potentially perilous[10]. How phagocytes adapt to continuous inhabitance in physiological hypoxic environments and how such adaptations inform efferocytosis remains unexplored. Here, we made the striking observation that macrophages conditioned in prolonged physiological hypoxia (~1% O_2) *in vitro* or *in vivo* are better phagocytes, both internalizing more ACs and degrading internalized ACs faster. As part of an adaptive response to prolonged physiological hypoxia, macrophages induce two distinct states that support efficient efferocytosis. The first state, which we term 'primed', is characterized by concomitant changes in mRNA and protein programs, especially metabolic programs, in AC-naïve macrophages that remain induced during efferocytosis. The second state, which we term 'poised', is characterized by transcription, but not translation, of phagocyte function programs (e.g., phagocytosis programs) in AC-naïve macrophages that are subsequently translated during efferocytosis. We found that both primed and poised state programs support enhanced continual efferocytosis by macrophages residing under chronic physiological hypoxia. Importantly, we found that this 'primed' state, in particular induction of a noncanonical pentose phosphate pathway loop that generates abundant NADPH, directly supports enhanced, continual efferocytosis (a core 'poised' state program). Based on our findings, we propose that phagocytes that reside in physiological hypoxic environments, such as highly phagocytic macrophages in the bone marrow or spleen[9,19], adopt distinct

states that both ensure their own fitness and their readiness to perform core homeostatic functions.

Previous analysis of phagocytosis in different oxygen levels has produced mixed findings. For instance, past studies have suggested that acute hypoxia enhances internalization of opsonized targets[46], bacteria[47,48], and ACs[19], whereas other studies have suggested that acute hypoxia has no effect on phagocytosis[48–50] or decreases clearance of ACs[51], and that macrophages in hypoxic regions may produce less of the anti-inflammatory mediatory IL-10 typically produced during efferocytosis[25]. Much of the contradiction might relate to variations in how hypoxia was induced/maintain or for how long cells were cultured in hypoxia, typically ranging from 3h to 24h. Indeed, significant cellular changes can occur, including degradation of HIF proteins and HIF-dependent transcriptional programs, as quickly as 24h after introduction to hypoxia[28,52]. Although we observed a modest increase in population-level efferocytosis in macrophages exposed to acute physiological hypoxia, these cells did not exhibit enhanced lysosomal degradation. Instead, the most dramatic differences in both uptake and degradation of ACs were observed in macrophages conditioned in chronic physiological hypoxia. It will be interesting to further interrogate the importance of prolonged physiological hypoxia, including identified ‘primed’ and ‘poised’ programs, especially considering phagocytes residing in physiologically hypoxic tissues are often responsible for clearing biological material beyond conventional ACs[8,10].

Despite the growing body of work detailing how cells undergo metabolic adaptation to chronic hypoxia, understanding how such changes inform cellular function remains largely unexplored. We move beyond a phenomenological understanding of cellular metabolic adaption to chronic physiological hypoxia by mechanistically linking the changes in macrophage metabolism to enhanced AC uptake and degradation. Unexpectedly, we found that macrophages under prolonged physiological hypoxia limit glucose flux to most major pathways including anaerobic glycolysis and the TCA cycle. Instead, macrophages shunt glucose into a noncanonical PPP loop involving repeated cycling of PPP intermediates back to G6P via a process resembling gluconeogenesis. We found that this PPP loop is necessary for generation of NADPH in AC-naïve macrophages and appears to provide the NADPH necessary for appropriate phagolysosomal maturation and AC degradation. The importance of the PPP for efficient efferocytosis was also recently independently demonstrated using the small molecule 6-AN *in vitro* and in the thymus *in vivo*[41,42]. Our results suggest that it is this noncanonical PPP loop, and not the canonical PPP per se, that is required in tissue-resident macrophages residing in physiological hypoxic tissues. Collectively, we speculate that the adaptations observed in our study represent normal physiology of tissue-resident macrophages residing in physiological hypoxic tissues.

Limitations of the study

A series of important questions arise from our work related to our observation that chronic physiological hypoxia seems to induce both ‘primed’ and ‘poised’ states in macrophages. For instance, what macrophage functions, beyond efferocytosis, are ‘poised’ under chronic physiological hypoxia? Efferocytosis is generally a core macrophage function shared across tissue-resident macrophage populations, but are there functions that are informed by a

combination of oxygen availability and tissue-specific factors (e.g., presence of heme)? Finally, how are these poised programs regulated, for example, are they maintained by ribosomal stalling or increased chromatin accessibility/transcription? Future studies are required to determine the answers to these questions and could provide important clues on how macrophage function in specific environments to maintain tissue homeostasis.

STAR Methods

RESOURCE AVAILABILITY

Lead contact—Further information and requests for resources and reagents should be directed to the Lead Contact, Justin S. A. Perry (perryj@mskcc.org).

Materials availability—This study did not generate new reagents or materials.

Data and code availability

- mRNA sequencing raw data files have been deposited in NCBI Gene Expression Omnibus (GEO) archive (accession GSE192969). An Excel file with plotted data points and a pdf image with uncropped western blots are in Data S1.
- No new code was used in the preparation of this manuscript.
- Any additional information required to reanalyze the data reported in this paper is available from the lead contact upon request.

EXPERIMENTAL MODEL AND SUBJECT DETAILS

Mice—Animals were housed at the Memorial Sloan Kettering Cancer Center (MSKCC) animal facility under specific pathogen free (SPF) conditions on a 12-hour light/dark cycle under ambient conditions with ad libitum access to food and water. All studies were approved by the Sloan Kettering Institute (SKI) Institutional Animal Care and Use Committee (IACUC).

Cell Lines and Primary Cells—Primary ER-Hoxb8 myeloid progenitors, Jurkat T lymphoma cells, MDA-MB-231 breast cancer cells, BrM2 metastatic breast cancer cells, and E0771 breast cancer cells were cultured in Dulbecco's Modified Eagle's Medium (DMEM) or Roswell Park Memorial Institute Medium (RPMI) supplemented with lot-tested 10% fetal bovine serum (FBS), 1mM L-glutamine, penicillin, and streptomycin. Cells were cultured at 37°C in a humidified 5% CO_2 standard oxygen (21%) or hypoxic (1%) cell incubator.

METHOD DETAILS

Standard Oxygen and Hypoxia Conditioning—To model standard oxygen, acute hypoxia, and chronic hypoxia environments, we optimized protocols using the BioSpherix Xvivo X3 system, which allows us to dynamically regulate CO_2 and O_2 (down to 0.1%) in four different chambers without exposing cells to atmosphere. Primary macrophage progenitors immortalized with a modified estrogen receptorHoxb8 fusion (ER-Hoxb8) were generated as previously reported[53] from C57BL/6J mice. Progenitors were maintained in RPMI 1640 containing 5% heat-inactivated fetal bovine serum, 5% P885L (GM-CSF

producing)-conditioned media, and 0.5μM β-estradiol (Sigma) in standard oxygen (~21% O_2). To differentiate into primary macrophages, progenitors were first washed three times with cold PBS to remove β-estradiol. Progenitors were then cultured in a-MEM containing 5% heat-inactivated fetal bovine serum, 1% PenicillinStreptomycin-Glutamine (100X), and 10% L929 (M-CSF producing)-conditioned media. On day 6 of differentiation, mature macrophages were replated in non-TC treated plates and cultured in either standard oxygen or hypoxia (1% O_2) for 7 days prior to use in efferocytosis assays. For some experiments, progenitors were instead cultured in standard oxygen or hypoxia for 7 days prior to differentiation and use in efferocytosis assays. In all cases, media was replenished every other day and cells were incubated @37°C.

Induction of Apoptosis—For thymocyte phagocytosis, thymi from 6-week-old mice were harvested and crushed between frosted slides to release thymocytes. Cells were then treated with dexamethasone (5ǪM) for 4 hours prior to downstream use. Jurkat T lymphoma, MDA-MB-231, BrM2, and E0771 cells, were induced to undergo apoptosis by treatment with 150mJ cm^{-2} (Jurkat cells) or 650mJ cm^{-2} ultraviolet C irradiation (Stratalinker) at ~5×10^6 cell density per 10cm non-TC treated dish. Then, cells were incubated for 4h, 8h, 16h, or 24h before downstream use. Apoptosis was confirmed via Annexin V/7-AAD staining to be greater than 70% Annexin V+ single-positive (Figure S1A).

In Vitro Efferocytosis Assays—Apoptotic cells were stained with either 1μM CypHer5E (Cytiva) or 50μM TAMRA-SE (ThermoFisher) in serum-free HBSS for 45min. Then, cells were washed by incubating in serum-containing assay media for an additional 25min. Apoptotic cells were co-cultured with macrophages at a 1:1 phagocyte to target ratio. All efferocytosis assays included four technical replicates for each condition with at least three biological replicates. For all pharmacological studies, phagocytes were pre-incubated with the compounds listed below or vehicle (DMSO) for 16h or 6d prior to addition of apoptotic cells. Macrophages were treated with the following: Cycloheximide (Chx; Sigma, 100μM), 6-AN (MedChemExpress, 100μM), G6PDi-1 (Cayman Chemical, 50μM), or FBP1i (Cayman Chemical, 25μM). Macrophages were examined via microscopy to ensure no gross morphological changes or cell death had occurred due to drug treatment. Macrophages and apoptotic cells were co-cultured for 1h. Apoptotic cells were subsequently removed via three washes with cold assay media and phagocytes were harvested using a cell scraper (Biotium) and assessed by flow cytometry. For continual efferocytosis, the first round of apoptotic cells was labeled with CFSE (ThermoFisher) and co-cultured with macrophages at a 1:1 ratio for 1h. Then, apoptotic cells were washed away using cold assay media. Macrophages were subsequently rested for 1.5h prior to co-culture with a second round of apoptotic cells that were labeled with CypHer5E. Continual efferocytosis was assessed by flow cytometry as CFSE+ (1st AC uptake) and CFSE+ CypHer5E+ (2nd AC uptake) macrophages. flow cytometry analysis was performed using an Attune NxT Flow Cytometer (ThermoFisher) and analyzed using FlowJo 10.7.1.

Time-lapse Confocal Microscopy

Equipment.: Experiments to evaluate per-cell uptake and degradation were performed on a Zeiss Axio Observer.Z1 7 inverted fluorescence microscope equipped with a Zeiss 20x

PlanApo (0.8 NA) objective, a 6-channel, 7-laser LSM 980 (405nm, 445nm, 488nm, 514nm, 561nm, 594nm, 639nm), and a Airyscan 2 multiplex detector. The imaging stage is fully encased in a black-out environmental chamber and the Z PIEZO stage is fully encapsulated with a heating/gas-controlled insert, together allowing us to control the temperature, humidity, CO_2, and O_2. Time-lapse experiments were acquired using Zen Blue software (Zeiss).

Experiment.: Prior to imaging, cells were allowed to acclimate for at least 10min. After selection of scenes (see below), apoptotic cells were added to phagocyte-containing chamber slides and scenes were rapidly focused prior to the beginning of data collection. For each condition/experiment, at least 8 regions ('scenes') were selected and imaged. Scenes were selected if they featured at least 10 cells per region, and when experimental manipulations were performed (e.g., 6-AN treatment), regions were selected that featured similar cell numbers between vehicle and treatment conditions. Scenes were imaged every 4min for a minimum of 8h per experiment, which generally equates to ~0.5μs per pixel or 5s per scene. Time-lapse experiments were performed in Multiplex CO-8Y mode which allows for gentle confocal-resolution imaging at a high frame rate. Specifically, we set the pinhole to 2.42 Airy units (57μm) with the image scaling (per pixel) set at 0.414μm × 0.414μm with 2x averaging. Focusing was ensured using the Definite Focus 2 module with a two-part strategy that was first based on the initial focus of individual scenes and then subsequently updated after each round of images. Analysis, including generation of scale bars, was performed using Zen Blue or Fiji.

Ex Vivo Efferocytosis—To perform ex vivo efferocytosis, tissues were isolated from 7-week-old female C57BL/6 mice. To isolate bone marrow-resident macrophages (BMMs), bone marrow was flushed from bones using a 25G needle with α-MEM media containing FBS in a hypoxia chamber set to 1% oxygen. Red blood cells were lysed, and remaining bone marrow cells were plated in a non-TC treated 6-well plate in BMDM media and cultured overnight in either hypoxia (1%) or standard (21%) oxygen. Floating cells were removed and fresh BMDM media was added. BMMs were then co-cultured with CypHer5E-labeled apoptotic MDA-MD-231 cells at a 1:1 ratio for 1h. Macrophages were isolated, stained with CD11b and F4/80, and analyzed via flow cytometry. To isolate splenic macrophages, spleens were minced into small pieces in a hypoxia chamber set to 1% oxygen and digested for 20min at 37C. Cell suspensions were strained using a 70μm cell strainer. Red blood cells were lysed, and remaining splenic cells were plated and treated identical to bone marrow-resident macrophages as described above.

In Vivo Efferocytosis—To perform *in vivo* efferocytosis, we performed two models: dexamethasone (Dex)-induced apoptotic thymocyte removal and peritoneal apoptotic T cell removal. For Dex-induced clearance, six- to eight-week-old mice were injected i.p. with 300μl PBS containing 250μg dexamethasone (50μM; Sigma) with or without cycloheximide (5mg/kg) or 6-AN (3mg/kg) dissolved in EtOH. 6h after injection, thymi were harvested from mice and the numbers of thymocytes with annexin V staining only (apoptotic) versus annexin V/7-AAD double positive cells (secondarily necrotic) were assessed via flow cytometry. For the peritoneal clearance model, Cas9+ macrophages

bearing either a scramble control guide or guides targeting G6pdx where initially conditioned in physiological hypoxia (1% O_2) for 7d. Conditioned macrophages were subsequently i.p. injected 1h prior to injection of apoptotic cells. Then, mice were injected with 1e6 CypHer5E-labeled apoptotic Jurkat T cells and allowed to rest. Mice were subsequently euthanized 1h post-injection. Peritoneal lavage was collected in 8ml cold PBS. Collected lavage was centrifuged and cells were blocked with CD16/32 (clone 24G2) prior to staining with CD11b (eBioscience, 48-0112-82, clone M1/70, 1:750) and F4/80 (eBioscience, 12-4801-82, clone BM8, 1:750) for 30min at 4°C. Efferocytosis was analyzed by quantifying CypHer5E+ events within the CD11b+ F4/80high macrophages via flow cytometry.

RNA Sequencing—For bulk RNA sequencing, 4.5×10^5 macrophages were conditioned for 7d in standard O_2 (~21%) and either immediately collected or pulsed with 3h of 1% O_2 (acute) and then collected. In parallel, 4.5×10^5 macrophages were conditioned for 7d in 1% O_2 (chronic) then collected. Collected samples were subsequently collected, washed with cold PBS, and lysed on ice with beta-mercaptoethanol-containing lysis buffer (Buffer RA, Machery-Nagel) for downstream RNA isolation. Total RNA was isolated using the NucleoSpin RNA isolation kit with on-column rDNase digestion (Machery-Nagel) and mRNA libraries were generated by polyA capture and reverse transcription of cDNA. Libraries were then sequenced at 150bp (paired-end) reads with ~20 million reads per sample using an Illumina NovaSeq 6000 sequencer.

Proteomics—For ^{13}C SILAC labeling, target cells were grown in lysine- and arginine-deficient DMEM with 10% dialyzed FBS, 1% PSQ, and 2mM L-glutamine, supplemented with ‘heavy’ $^{13}C_6$-lysine and ‘light’ $^{12}C_6$-arginine (100mg/L; Cambridge Isotope Laboratories). After 8–10 passages, incorporation of $^{13}C_6$-lysine-labeled amino acids into proteins was verified via LC-MS/MS to be >99%. Heavy isotope-labeled target cells were expanded in $^{13}C_6$-lysine media and induced to undergo apoptosis. Macrophages were first conditioned in standard oxygen or hypoxia (see above), and then cultured with or without apoptotic cells for 1h. Apoptotic cells were subsequently removed using two cold assay media washes and two cold PBS washes. Macrophages were then removed using a cell scraper, pelleted to remove any residual liquid, and immediately snap frozen on dry ice.

Sample Preparation.: Cell pellets were lysed with 200–300μL buffer containing 8M urea and 200mM EPPS (pH at 8.5) with protease inhibitor (Roche) and phosphatase inhibitor cocktails 2 and 3 (Sigma). Lysates were aspirated 2x on ice, followed by water sonication for 2min @4°C. Benzonase (Millipore) was added to a concentration of 50u/mL and incubated on ice for 15min. Samples were centrifuged at 14,000g for 10 min (@4°C) and the supernatant was subsequently extracted. The Pierce bicinchoninic acid (BCA) protein concentration assay was used to determine protein concentration. Protein disulfide bonds were reduced with 5mM tris (2-carboxyethyl) phosphine (@RT, 30min), then alkylated with 10mM iodoacetamide (@RT, 30min, in the dark). The reaction was quenched with 10mM dithiothreitol (@RT, 15min). Equivalent volumes of lysate aliquots were taken for each sample (100–200μg in each sample) and diluted to approximately 100μL with lysis buffer. Samples were subjected to methanol for 5s, then chloroform was added for

an additional 5s prior to centrifugation and precipitation[54]. Pellets were reconstituted in 100μL of 200mM EPPS buffer and digested with Lys-C (1:100 enzyme-to-protein ratio) and incubated @37°C for 4h. Trypsin was then added (1:100 enzyme-to-protein ratio) and digested @37°C overnight. Anhydrous acetonitrile was then added to make a final volume of 30% ACN.

TMT Labeling.: Samples were TMT-labeled as described[54]. Briefly, samples were TMT-tagged by adding 10μL (28μg/μL) of TMTPro reagent for each sample and incubated for 1h @RT. A ratio check was performed by taking a 2μL aliquot from each sample and desalted by the StageTip method[55] to confirm labeling efficiency. TMT-tags were then quenched with hydroxylamine to a final concentration of 0.3% for 15min @RT. Samples were pooled in their entirety, then dried via vacuum-centrifugation. Dried samples were reconstituted in 1mL of 3% ACN/1% TFA, desalted using a 100mg tC18 SepPak (Waters), and lyophilized overnight. Lyophilized peptides were dried using vacuum-centrifugation and reconstituted in 1mL of 2% ACN/25mM ABC. Peptides were fractionated into 48 fractions. Next, an Ultimate 3000 HPLC (Dionex) coupled to an Ultimate 3000 Fraction Collector using a Waters XBridge BEH130 C18 column (3.5μm × 4.6mm × 250mm) was operated at 1mL/min. The Buffers A, B, and C used below consisted of 100% water, 100% ACN, and 25mM ABC, respectively. The fractionation gradient operated as follows: 1% B to 5% B in 1min, 5% B to 35% B in 61min, 35% B to 60% B in 5min, 60% B to 70% B in 3min, 70% B to 1% B in 10min, with 10% C the entire gradient to maintain pH. The 48 fractions were then concatenated to 12 fractions (i.e., fractions 1, 13, 25, 37 were pooled, followed by fractions 2, 14, 26, 38, etc.) so that every 12th fraction was used to pool. Pooled fractions were vacuum-centrifuged then reconstituted in 1% ACN/0.1% FA for LCMS/MS.

LC-MS/MS.: Total fractions were analyzed by LC-MS/MS using a NanoAcquity (Waters) with a 50cm EASY-Spray Column (PepMap RSLC, C18, 2μm, 100Å, 75μm I.D.) heated to 60°C coupled to a Orbitrap Eclipse Tribrid Mass Spectrometer (Thermo Fisher Scientific). Peptides were separated by direct inject at a flow rate of 300nL/min using a gradient of 5 to 30% acetonitrile (0.1% FA) in water (0.1% FA) over 3h then to 50% ACN in 30min and analyzed by SPS-MS3. MS1 scans were acquired over a range of m/z 375–1500, 120K resolution, AGC target (4.0e5), and maximum IT of 50ms. MS2 scans were acquired on MS1 scans of charge 2–7 using an isolation of 0.7m/z, collision induced dissociation with activation of 32%, turbo scan and max IT of 50ms. MS3 scans were acquired using specific precursor selection (SPS) of 10 isolation notches, m/z range 100–1000, 50K resolution, AGC target (1.0e5), HCD activation of 45%, and max IT of 150ms. The dynamic exclusion was set at 60s.

TMT Data Analysis.: Raw data files were processed using Proteome Discoverer (PD) version 2.4.1.15 (Thermo Scientific). For each of the TMT experiments, raw files from all fractions were merged and searched with the SEQUEST HT search engine with a UniProt protein database downloaded on 2019/01/09 (176,945 entries). The precursor and fragment mass tolerances were 10ppm and 0.6Da respectively. A maximum of two trypsin missed cleavages were permitted. Searches used a reversed sequence decoy strategy to control peptide false discovery rate (FDR) and 1% FDR was set as threshold for identification.

Analysis of Nutrient Consumption and Secretion via YSI—Macrophages (2.5×10^6) were cultured in either standard oxygen or hypoxia (1% O_2) and conditioned for a total of 7 days. Media was changed at day 1, day 3, and day 5 prior to a 24h period of conditioning. At the end of the 24h period (denoted as day 2–3, day 4–5, and day 6–7 periods), media was collected, spun down to remove cell debris, and immediately snap frozen for downstream analysis via a 2950D Biochemistry Analyzer (YSI Life Sciences) to determine glucose and lactate concentrations. Absolute rates of consumption (glucose) or secretion (lactate) were calculated first by subtracting the concentration observed in control (cell-free) media incubated in parallel, then normalized to cell number and volume of media. These experiments were performed independently at least two times.

Untargeted Metabolomics—Macrophages (2.5×10^6) were conditioned in standard oxygen or hypoxia for 7d. To protect from experimental artifact, all samples were collected in the same oxygen environment that they were conditioned in. Plates containing cells were placed on ice and washed with cold PBS three times, then moved to dry ice and ice cold 80% methanol was added. Cells were subsequently scraped and transferred to a cold centrifuge tube on dry ice. The cell-methanol slurries were then vortexed for 1min, allowed to rest on dry ice for 5min, then vortexed an additional 1min to create cell lysates. Lysates were centrifuged for 20min at 14,000g in a refrigerated centrifuge set to 4°C to remove debris. Supernatants were transferred to clean tubes and lyophilized in the absence of heat and dissolved in water. Targeted LC/MS analyses were performed on a Q Exactive Orbitrap mass spectrometer (Thermo Scientific) coupled to a Vanquish UPLC system (Thermo Scientific). The Q Exactive operated in polarity-switching mode. A Sequant ZIC-HILIC column (2.1mm i.d. × 150mm, Merck) was used for separation of metabolites. Flow rate was set at 150μL/min. Buffers consisted of 100% acetonitrile for mobile B, and 0.1% NH4OH/ 20mM CH3COONH4 in water for mobile A. Gradient ran from 85% to 30% B in 20min followed by a wash with 30% B and re-equilibration at 85% B. MS data were processed using Compound Discoverer (Thermo Scientific). An in-house metabolite library as well as Chemspider were searched for metabolite identification. Three levels of metabolite identification were reported: 1) identified compounds: definitive identification based on the mass (within 5ppm) and retention time of authentic chemical standards; 2) putatively annotated compounds by searching ChemSpider (mass tolerance 5ppm); 3) compounds with predicted chemical composition based on mass. Relative metabolite quantitation was performed based on peak area for each metabolite. Hierarchical clustering analysis and principal component analysis (PCA) were performed by Compound Discoverer (Thermo Scientific).

^{13}C-Metabolic Flux Analysis—Experiments were performed similar to those outlined in Untargeted Metabolomics with the following modification. On day 5, glucose-deficient RPMI containing 1 g/L [1,2-^{13}C]-glucose or [U-^{13}C]-glucose (both from Cambridge Isotope Laboratories), 10% L929-conditioned media, 1% PSQ, and 10% FBS was conditioned in either standard oxygen or hypoxia for 16–24h. On day 6, conditioned macrophages were washed with PBS twice and then cultured with heavy isotope-containing media for 16h. Metabolites were extracted using the same protocol detailed in Untargeted Metabolomics. LC/MS analyses were performed on a Q Exactive Orbitrap mass spectrometer (Thermo

Scientific) coupled to a Vanquish UPLC system (Thermo Scientific). The Q Exactive operated in polarity-switching mode. A Sequant ZIC-HILIC column (2.1mm i.d. × 150mm, Merck) was used for separation of metabolites. Flow rate was set at 150μL/min. Buffers consisted of 100% acetonitrile for mobile B, and 0.1% NH4OH/20mM CH3COONH4 in water for mobile A. Gradient ran from 85% to 30% B in 20min followed by a wash with 30% B and re-equilibration at 85% B. Data analysis was done using El-MAVEN (v0.12.0). Metabolites and their ^{13}C isotopologues were identified on the basis of exact mass within 5ppm and standard retention times. Relative metabolite quantitation was performed based on peak area for each metabolite.

Analysis of Mitochondrial Properties—For analysis of mitochondrial superoxide levels, conditioned macrophages were labeled with the live cell-permeant fluorogenic probe MitoSOX Red (ThermoFisher). MitoSOX Red is targeted to the mitochondria and is oxidized by superoxide but not reactive oxygen or nitrogen species, inducing an increase in fluorescence which we quantified using flow cytometry. To estimate mitochondrial shape and content, conditioned macrophages were labeled with both MitoTracker Green (MTG) and MitoTracker Deep Red (MTDR, both ThermoFisher). MTG localizes to mitochondria independent of mitochondrial membrane potential whereas MTDR labeling of mitochondria is dependent on mitochondrial membrane potential. Combined, the two fluorogenic probes were used to estimate potential and quantity (via flow cytometry).

NADP+/NADPH, ATP, and GSH/GSSG Measurement—4×10^6 or 2.5×10^4 (for GSH/GSSG) macrophages were seeded for conditioning and subsequent NADP+/NADPH, ATP, or GSH/GSSG measurement. In some experiments, macrophages were treated with 6-AN (100nM) or vehicle (DMSO) beginning one day after replating. On day 7, cells were collected, processed, and the ratio of NADP+/NADPH or GSH/GSSG was measure using the NADP/NADPH Quantitation Colorimetric Kit (BioVision) or the GSH/GSSG-Glo Assay (Promega), respectively, or ATP was quantitated using the Luminescent ATP Detection Assay Kit (Abcam), following the manufacturer's protocol.

Measurement of Redox State and Lysosomal Acidity—Lipid peroxidation and cellular ROS was determined by labeling of phagocytes using the reagent BODIPY 581/591 C11 and CellROX Deep Red (both ThermoFisher), respectively, followed by flow cytometric analysis. Lysosomal acidity was determined by labeling of phagocytes using the reagent Lysosensor Green DND-189 (ThermoFisher). Labeling was performed according to manufacturer instructions. For analysis of redox state or lysosomal acidity in efferocytotic cells, phagocytes were first gated on CypHer5E+.

CRISPR/Cas9 Deletion or siRNA knockdown of SLCs—Stable, individual clones of Cas9-expressing Hoxb8 macrophages were generated using bone marrow from Cas9 mice (JAX Strain #026179) and a lentiviral transduction protocol adapted from Fang Zhang and colleagues. *G6pdx* was disrupted using the Zhang lab lentiGuide-Puro sgRNA plasmid with a verified guide for *G6pdx*. lentiGuide-Puro was a gift from Feng Zhang (Addgene plasmid # 52963). Guide RNAs targeting *G6pdx* and scramble control were generated using the following oligo pairs:

G6pdx:

5’---CACCGACCTGAAGATACCTTCATTG-−-3’

5’---AAACCAATGAAGGTATCTTCAGGTC-−-3’

Scramble Control:

5’--- CACCGCACTCACATCGCTACATCA-−-3’

3’--- AAACTGATGTAGCGATGTGAGTGC-−-5’.

QUANTIFICATION AND STATISTICAL ANALYSIS

Statistical analyses were executed using GraphPad Prism 7, SPSS v.22, and R v.4.0.5. We determined statistical significance, depending on the structure of the data, via unpaired two-tailed Student’s t-test, nonparametric Mann–Whitney U-test, one-way or two-way ANOVA, or Fisher’s exact test. The statistical test used for each experiment can be found in the corresponding figure legend. R v.4.0.5 was used for graphical and statistical analyses and the R package DESeq2 was used for differential gene expression analysis of transcriptomic and proteomic analyses. All genes were curated according to a previously described approach[21]. Briefly, complementary analyses of biological pathways were performed by comparing significantly differentially expressed genes or proteins and cross-referencing them with the Molecular Signatures Database (MSigDB). Gephi (v.0.9.1 https://gephi.org/) was used to perform standard network clustering analyses. The “Link Communities” algorithm for biological network analysis was used to calculate edges and nodes[56]. The Yifan Hu layout algorithm was used to determine network structure. All biologically independent samples were included and used for statistical and graphical analyses. No data was excluded from this manuscript and can be found online under Data S1 - Source Data. Sample sizes were not predetermined using statistical methods. RNA sequencing data is deposited under NCBI GEO accession GSE192969.

Supplementary Material

Refer to Web version on PubMed Central for supplementary material.

Acknowledgements

We thank members of the Perry laboratory and co-authors for edits and discussions related to this manuscript. We thank Justin Cross and the Donald B. and Catherine C. Marron Cancer Metabolism Center at MSKCC for help with YSI experiments. This work was supported by grants to J.S.A.P. from the NIH (NCI 5R00CA237728; NIGMS 1DP2GM146337), a Parker Institute for Cancer Immunotherapy Career Development Award, a V Foundation Scholars Award, a MSKCC Functional Genomics Institute pilot award, a grant to K.R.K. from the NIH (NCI 1R01CA248364), and MSKCC Cancer Center Support Grant P30CA008748. Some figure panels were created using the commercial version of BioRender.

References

1. Boada-Romero E, Martinez J, Heckmann BL, and Green DR (2020). The clearance of dead cells by efferocytosis. Nature Reviews Molecular Cell Biology 21, 398–414. 10.1038/s41580-020-0232-1. [PubMed: 32251387]

2. Doran AC, Yurdagul A, and Tabas I (2020). Efferocytosis in health and disease. Nature Reviews Immunology 20, 254–267. 10.1038/s41577-019-0240-6.

3. Rothlin CV, Hille TD, and Ghosh S (2020). Determining the effector response to cell death. Nat Rev Immunol. 10.1038/s41577-020-00456-0.

4. Elliott Michael R., and Ravichandran Kodi S. (2016). The Dynamics of Apoptotic Cell Clearance. Developmental Cell 38, 147–160. 10.1016/j.devcel.2016.06.029. [PubMed: 27459067]

5. Henson PM (2017). Cell Removal: Efferocytosis. Annual Review of Cell and Developmental Biology 33, 127–144. 10.1146/annurev-cellbio-111315-125315.

6. Morioka S, Maueröder C, and Ravichandran KS (2019). Living on the Edge: Efferocytosis at the Interface of Homeostasis and Pathology. Immunity 50, 1149–1162. 10.1016/j.immuni.2019.04.018. [PubMed: 31117011]

7. Penberthy KK, Lysiak JJ, and Ravichandran KS (2018). Rethinking Phagocytes: Clues from the Retina and Testes. Trends Cell Biol 28, 317–327. 10.1016/j.tcb.2018.01.004. [PubMed: 29454661]

8. Zago G, Saavedra PHV, Keshari KR, and Perry JSA (2021). Immunometabolism of Tissue-Resident Macrophages – An Appraisal of the Current Knowledge and Cutting-Edge Methods and Technologies. Frontiers in Immunology 12. 10.3389/fimmu.2021.665782.

9. Sender R, and Milo R (2021). The distribution of cellular turnover in the human body. Nature Medicine 27, 45–48. 10.1038/s41591-020-01182-9.

10. Trzeciak A, Wang Y-T, and Perry JSA (2021). First we eat, then we do everything else: The dynamic metabolic regulation of efferocytosis. Cell Metabolism. 10.1016/j.cmet.2021.08.001.

11. Amit I, Winter DR, and Jung S (2016). The role of the local environment and epigenetics in shaping macrophage identity and their effect on tissue homeostasis. Nature Immunology 17, 18–25. 10.1038/ni.3325. [PubMed: 26681458]

12. Guilliams M, and Svedberg FR (2021). Does tissue imprinting restrict macrophage plasticity? Nature Immunology 22, 118–127. 10.1038/s41590-020-00849-2. [PubMed: 33462453]

13. Guilliams M, Thierry GR, Bonnardel J, and Bajenoff M (2020). Establishment and Maintenance of the Macrophage Niche. Immunity 52, 434–451. 10.1016/j.immuni.2020.02.015. [PubMed: 32187515]

14. Okabe Y, and Medzhitov R (2016). Tissue biology perspective on macrophages. Nature Immunology 17, 9–17. 10.1038/ni.3320. [PubMed: 26681457]

15. Blériot C, Chakarov S, and Ginhoux F (2020). Determinants of Resident Tissue Macrophage Identity and Function. Immunity 52, 957–970. 10.1016/j.immuni.2020.05.014. [PubMed: 32553181]

16. Breed ER, Watanabe M, and Hogquist KA (2019). Measuring Thymic Clonal Deletion at the Population Level. Journal of immunology (Baltimore, Md. : 1950) 202, 3226–3233. 10.4049/jimmunol.1900191. [PubMed: 31010850]

17. Stritesky GL, Xing Y, Erickson JR, Kalekar LA, Wang X, Mueller DL, Jameson SC, and Hogquist KA (2013). Murine thymic selection quantified using a unique method to capture deleted T cells. Proceedings of the National Academy of Sciences of the United States of America 110, 4679–4684. 10.1073/pnas.1217532110. [PubMed: 23487759]

18. Carreau A, El Hafny-Rahbi B, Matejuk A, Grillon C, and Kieda C (2011). Why is the partial oxygen pressure of human tissues a crucial parameter? Small molecules and hypoxia. J Cell Mol Med 15, 1239–1253. 10.1111/j.1582-4934.2011.01258.x. [PubMed: 21251211]

19. Norris PC, Libreros S, and Serhan CN (2019). Resolution metabolomes activated by hypoxic environment. 5, eaax4895. doi:10.1126/sciadv.aax4895.

20. Trayhurn P (2019). Oxygen-A Critical, but Overlooked, Nutrient. Front Nutr 6, 10–10. 10.3389/fnut.2019.00010. [PubMed: 30809528]

21. Morioka S, Perry JSA, Raymond MH, Medina CB, Zhu Y, Zhao L, Serbulea V, Onengut-Gumuscu S, Leitinger N, Kucenas S, et al. (2018). Efferocytosis induces a novel SLC program to promote glucose uptake and lactate release. Nature 563, 714–718. 10.1038/s41586-018-0735-5. [PubMed: 30464343]

22. Perry JSA, Morioka S, Medina CB, Iker Etchegaray J, Barron B, Raymond MH, Lucas CD, Onengut-Gumuscu S, Delpire E, and Ravichandran KS (2019). Interpreting an apoptotic corpse

as anti-inflammatory involves a chloride sensing pathway. Nature Cell Biology 21, 1532–1543. 10.1038/s41556-019-0431-1. [PubMed: 31792382]

23. Wang Y, Subramanian M, Yurdagul A, Barbosa-Lorenzi VC, Cai B, de Juan-Sanz J, Ryan TA, Nomura M, Maxfield FR, and Tabas I (2017). Mitochondrial Fission Promotes the Continued Clearance of Apoptotic Cells by Macrophages. Cell 171, 331–345.e322. 10.1016/j.cell.2017.08.041. [PubMed: 28942921]
24. Yurdagul A, Subramanian M, Wang X, Crown SB, Ilkayeva OR, Darville L, Kolluru GK, Rymond CC, Gerlach BD, Zheng Z, et al. (2020). Macrophage Metabolism of Apoptotic Cell-Derived Arginine Promotes Continual Efferocytosis and Resolution of Injury. Cell Metabolism 31, 518–533.e510. 10.1016/j.cmet.2020.01.001. [PubMed: 32004476]
25. Zhang S, Weinberg S, DeBerge M, Gainullina A, Schipma M, Kinchen JM, Ben-Sahra I, Gius DR, Yvan-Charvet L, Chandel NS, et al. (2019). Efferocytosis Fuels Requirements of Fatty Acid Oxidation and the Electron Transport Chain to Polarize Macrophages for Tissue Repair. Cell Metabolism 29, 443–456.e445. 10.1016/j.cmet.2018.12.004. [PubMed: 30595481]
26. Park D, Han CZ, Elliott MR, Kinchen JM, Trampont PC, Das S, Collins S, Lysiak JJ, Hoehn KL, and Ravichandran KS (2011). Continued clearance of apoptotic cells critically depends on the phagocyte Ucp2 protein. Nature 477, 220–224. 10.1038/nature10340. [PubMed: 21857682]
27. Viaud M, Ivanov S, Vujic N, Duta-Mare M, Aira L-E, Barouillet T, Garcia E, Orange F, Dugail I, Hainault I, et al. (2018). Lysosomal Cholesterol Hydrolysis Couples Efferocytosis to Anti-Inflammatory Oxysterol Production. Circulation research 122, 1369–1384. doi:10.1161/CIRCRESAHA.117.312333. [PubMed: 29523554]
28. Jain IH, Calvo SE, Markhard AL, Skinner OS, To T-L, Ast T, and Mootha VK (2020). Genetic Screen for Cell Fitness in High or Low Oxygen Highlights Mitochondrial and Lipid Metabolism. Cell 181, 716–727.e711. 10.1016/j.cell.2020.03.029. [PubMed: 32259488]
29. Hale LP, Braun RD, Gwinn WM, Greer PK, and Dewhirst MW (2002). Hypoxia in the thymus: role of oxygen tension in thymocyte survival. 282, H1467–H1477. 10.1152/ajpheart.00682.2001.
30. Denko NC (2008). Hypoxia, HIF1 and glucose metabolism in the solid tumour. Nature Reviews Cancer 8, 705–713. 10.1038/nrc2468. [PubMed: 19143055]
31. Sadiku P, and Walmsley SR (2019). Hypoxia and the regulation of myeloid cell metabolic imprinting: consequences for the inflammatory response. EMBO Rep 20, e47388. 10.15252/embr.201847388. [PubMed: 30872317]
32. Taylor CT, and Colgan SP (2017). Regulation of immunity and inflammation by hypoxia in immunological niches. Nature Reviews Immunology 17, 774–785. 10.1038/nri.2017.103.
33. Jang C, Chen L, and Rabinowitz JD (2018). Metabolomics and Isotope Tracing. Cell 173, 822–837. 10.1016/j.cell.2018.03.055. [PubMed: 29727671]
34. Artyomov MN, and Van den Bossche J (2020). Immunometabolism in the Single-Cell Era. Cell Metabolism 32, 710–725. 10.1016/j.cmet.2020.09.013. [PubMed: 33027638]
35. Makowski L, Chaib M, and Rathmell JC (2020). Immunometabolism: From basic mechanisms to translation. 295, 5–14. 10.1111/imr.12858.
36. Ryan DG, and O'Neill LAJ (2020). Krebs Cycle Reborn in Macrophage Immunometabolism. Annual review of immunology 38, 289–313. 10.1146/annurev-immunol-081619-104850.
37. Cheng M-L, Lin J-F, Huang C-Y, Li G-J, Shih L-M, Chiu DT-Y, and Ho H-Y (2019). Sedoheptulose-1,7-bisphospate Accumulation and Metabolic Anomalies in Hepatoma Cells Exposed to Oxidative Stress. Oxidative Medicine and Cellular Longevity 2019, 5913635. 10.1155/2019/5913635. [PubMed: 30755786]
38. Longenecker JP, and Williams JF (1980). Quantitative measurement of the L-type pentose phosphate cycle with [2–14C]glucose and [5–14C]glucose in isolated hepatocytes. The Biochemical journal 188, 859–865. 10.1042/bj1880859. [PubMed: 7470039]
39. Williams JF, Blackmore PF, and Arora KK (1985). The significance of sedoheptulose 1,7-bisphosphate in the metabolism and regulation of the pentose pathway in liver. Biochemistry international 11, 599–610. [PubMed: 4084320]
40. Muri J, and Kopf M (2020). Redox regulation of immunometabolism. Nature Reviews Immunology. 10.1038/s41577-020-00478-8.

41. Tsai TL, Zhou TA, Hsieh YT, Wang JC, Cheng HK, Huang CH, Tsai PY, Fan HH, Feng HK, Huang YC, et al. (2022). Multiomics reveal the central role of pentose phosphate pathway in resident thymic macrophages to cope with efferocytosis-associated stress. Cell Rep 40, 111065. 10.1016/j.celrep.2022.111065. [PubMed: 35830797]

42. He D, Mao Q, Jia J, Wang Z, Liu Y, Liu T, Luo B, and Zhang Z (2021). Pentose Phosphate Pathway Regulates Tolerogenic Apoptotic Cell Clearance and Immune Tolerance. Front Immunol 12, 797091. 10.3389/fimmu.2021.797091. [PubMed: 35082786]

43. Bagaitkar J, Huang J, Zeng MY, Pech NK, Monlish DA, Perez-Zapata LJ, Miralda I, Schuettpelz LG, and Dinauer MC (2018). NADPH oxidase activation regulates apoptotic neutrophil clearance by murine macrophages. Blood 131, 2367–2378. 10.1182/blood-2017-09-809004 %J Blood. [PubMed: 29618478]

44. Mantegazza AR, Savina A, Vermeulen M, Pérez L, Geffner J, Hermine O, Rosenzweig SD, Faure F, and Amigorena S (2008). NADPH oxidase controls phagosomal pH and antigen cross-presentation in human dendritic cells. Blood 112, 4712–4722. 10.1182/blood-2008-01-134791 %J Blood. [PubMed: 18682599]

45. Yvan-Charvet L, Pagler TA, Seimon TA, Thorp E, Welch CL, Witztum JL, Tabas I, and Tall AR (2010). ABCA1 and ABCG1 Protect Against Oxidative Stress–Induced Macrophage Apoptosis During Efferocytosis. 106, 1861–1869. doi:10.1161/CIRCRESAHA.110.217281.

46. Acosta-Iborra B, Elorza A, Olazabal IM, Martín-Cofreces NB, Martin-Puig S, Miró M, Calzada MJ, Aragonés J, Sánchez-Madrid F, and Landázuri MO (2009). Macrophage oxygen sensing modulates antigen presentation and phagocytic functions involving IFN-gamma production through the HIF-1 alpha transcription factor. Journal of immunology (Baltimore, Md. : 1950) 182, 3155–3164. 10.4049/jimmunol.0801710. [PubMed: 19234213]

47. Anand RJ, Gribar SC, Li J, Kohler JW, Branca MF, Dubowski T, Sodhi CP, and Hackam DJ (2007). Hypoxia causes an increase in phagocytosis by macrophages in a HIF-1α-dependent manner. 82, 1257–1265. 10.1189/jlb.0307195.

48. Fritzenwanger M, Jung C, Goebel B, Lauten A, and Figulla HR (2011). Impact of short-term systemic hypoxia on phagocytosis, cytokine production, and transcription factor activation in peripheral blood cells. Mediators Inflamm 2011, 429501–429501. 10.1155/2011/429501. [PubMed: 21765619]

49. Dehn S, DeBerge M, Yeap X-Y, Yvan-Charvet L, Fang D, Eltzschig HK, Miller SD, and Thorp EB (2016). HIF-2α in Resting Macrophages Tempers Mitochondrial Reactive Oxygen Species To Selectively Repress MARCO-Dependent Phagocytosis. 197, 3639–3649. 10.4049/jimmunol.1600402 %J The Journal of Immunology.

50. Lin N, Shay JES, Xie H, Lee DSM, Skuli N, Tang Q, Zhou Z, Azzam A, Meng H, Wang H, et al. (2018). Myeloid Cell Hypoxia-Inducible Factors Promote Resolution of Inflammation in Experimental Colitis. Frontiers in Immunology 9. 10.3389/fimmu.2018.02565.

51. Marsch E, Theelen TL, Demandt JA, Jeurissen M, van Gink M, Verjans R, Janssen A, Cleutjens JP, Meex SJ, Donners MM, et al. (2014). Reversal of hypoxia in murine atherosclerosis prevents necrotic core expansion by enhancing efferocytosis. Arteriosclerosis, thrombosis, and vascular biology 34, 2545–2553. 10.1161/atvbaha.114.304023. [PubMed: 25256233]

52. Ginouvès A, Ilc K, Macías N, Pouysségur J, and Berra E (2008). PHDs overactivation during chronic hypoxia "desensitizes" HIFα and protects cells from necrosis. 105, 4745–4750. 10.1073/pnas.0705680105 %J Proceedings of the National Academy of Sciences.

53. Wang GG, Calvo KR, Pasillas MP, Sykes DB, Häcker H, and Kamps MP (2006). Quantitative production of macrophages or neutrophils ex vivo using conditional Hoxb8. Nature Methods 3, 287. 10.1038/nmeth865 https://www.nature.com/articles/nmeth865#supplementary-information. [PubMed: 16554834]

54. Navarrete-Perea J, Yu Q, Gygi SP, and Paulo JA (2018). Streamlined Tandem Mass Tag (SL-TMT) Protocol: An Efficient Strategy for Quantitative (Phospho)proteome Profiling Using Tandem Mass Tag-Synchronous Precursor Selection-MS3. Journal of Proteome Research 17, 2226–2236. 10.1021/acs.jproteome.8b00217. [PubMed: 29734811]

55. Rappsilber J, Mann M, and Ishihama Y (2007). Protocol for micro-purification, enrichment, pre-fractionation and storage of peptides for proteomics using StageTips. Nature Protocols 2, 1896–1906. 10.1038/nprot.2007.261. [PubMed: 17703201]

56. Ahn Y-Y, Bagrow JP, and Lehmann S (2010). Link communities reveal multiscale complexity in networks. Nature 466, 761–764. 10.1038/nature09182. [PubMed: 20562860]

Highlights

- Chronic physiological hypoxia enhances macrophage apoptotic cell uptake and degradation
- Chronic physiological hypoxia induces both primed and poised states in macrophages
- Both primed and poised state programs directly support enhanced continual efferocytosis
- A noncanonical PPP loop supports enhanced efferocytosis and maintains redox homeostasis

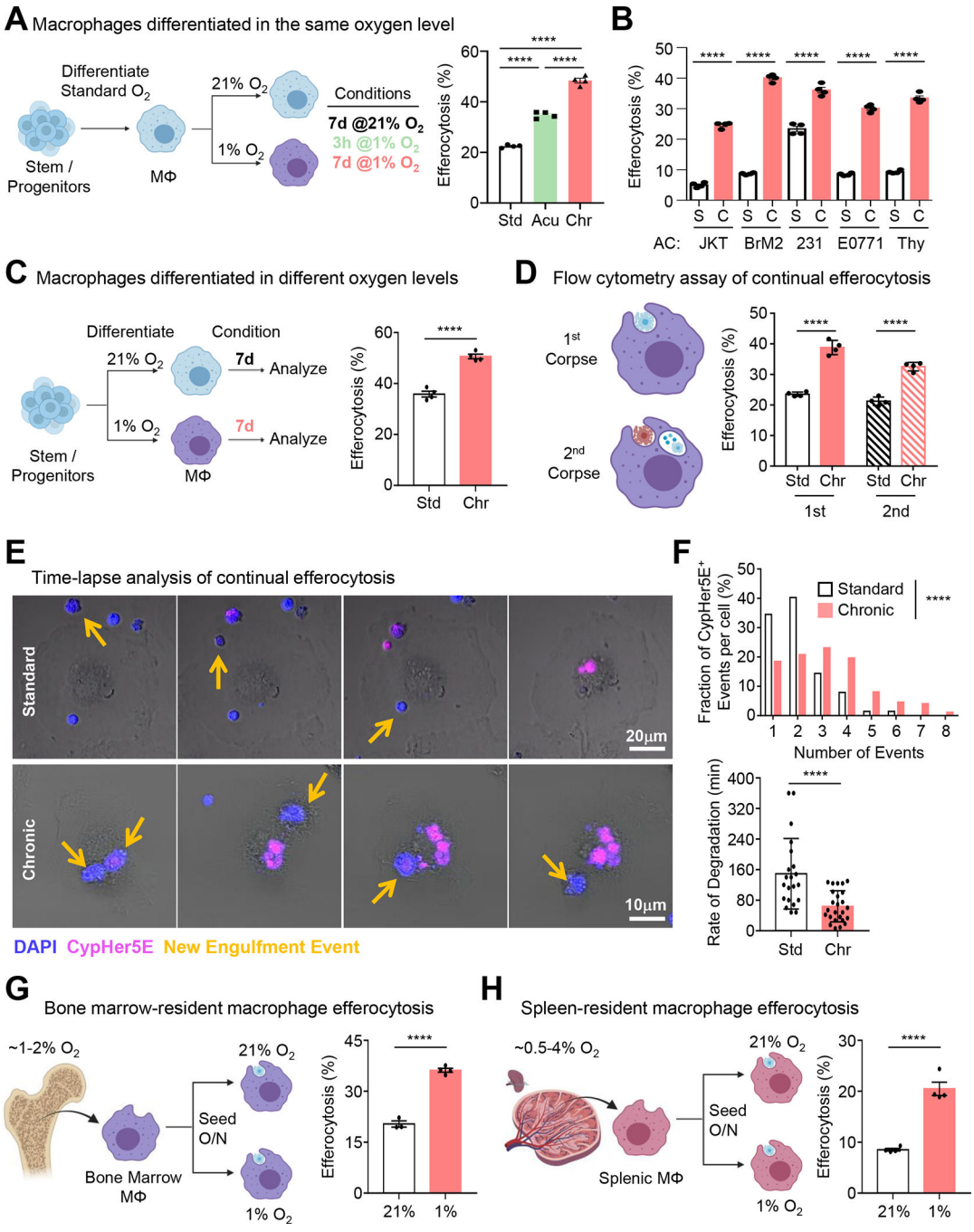

Figure 1: Efferocytosis is enhanced under prolonged ('chronic') physiological hypoxia

(A) Conditioned macrophages (left) were co-cultured with CypHer5E-labeled apoptotic MDA-MB-231s for 1h, then assessed via flow cytometry. Data are from four independent experiments, shown as mean ± SEM.

(B) Experiments performed as in (A), with the following targets: Jurkats, BrM2s, MDA-MD-231s, E0771s, and thymocytes. Data are from four independent experiments, shown as mean ± SEM.

(C) Conditioned macrophages (left) were co-cultured with CypHer5E-labeled apoptotic MDA-MB-231s for 1h, then assessed via flow cytometry. Data are from three independent experiments, shown as mean ± SEM.
(D) Experiments performed as in (A) but used to assess continual efferocytosis. Data are from three independent experiments, shown as mean ± SEM.
(E, F) Experiments performed as in (A), but imaged via time-lapse confocal microscopy. Yellow arrows indicate newly internalized ACs. (F) Quantification of CypHer5E+ events (top) and rate of degradation of internalized ACs (bottom). For quantification, 115 efferocytotic macrophages from 8 standard oxygen scenes and 155 efferocytotic macrophages from 6 chronic hypoxia scenes were analyzed. Data were binned as number of events per-cell and presented as a fraction of 100%. For analysis of degradation rate, 21 (standard oxygen) and 25 (chronic hypoxia) efferocytotic macrophages were analyzed. Degradation time = time to shrink internalized AC 50% after acidification (CypHer5E+).
(G, H) Bone marrow (G) or splenic (H) macrophages were isolated and seeded at either 1% or 21% oxygen overnight, then co-cultured with CypHer5E-labeled apoptotic MDA-MD-231 cells for 1h. Efferocytosis was assessed via flow cytometry. Data are from four independent experiments, shown as mean ± SEM.
Significance was determined by Student’s t-test in C,F-H, and by one-way ANOVA in A,B,D,F, ****p < .0001.

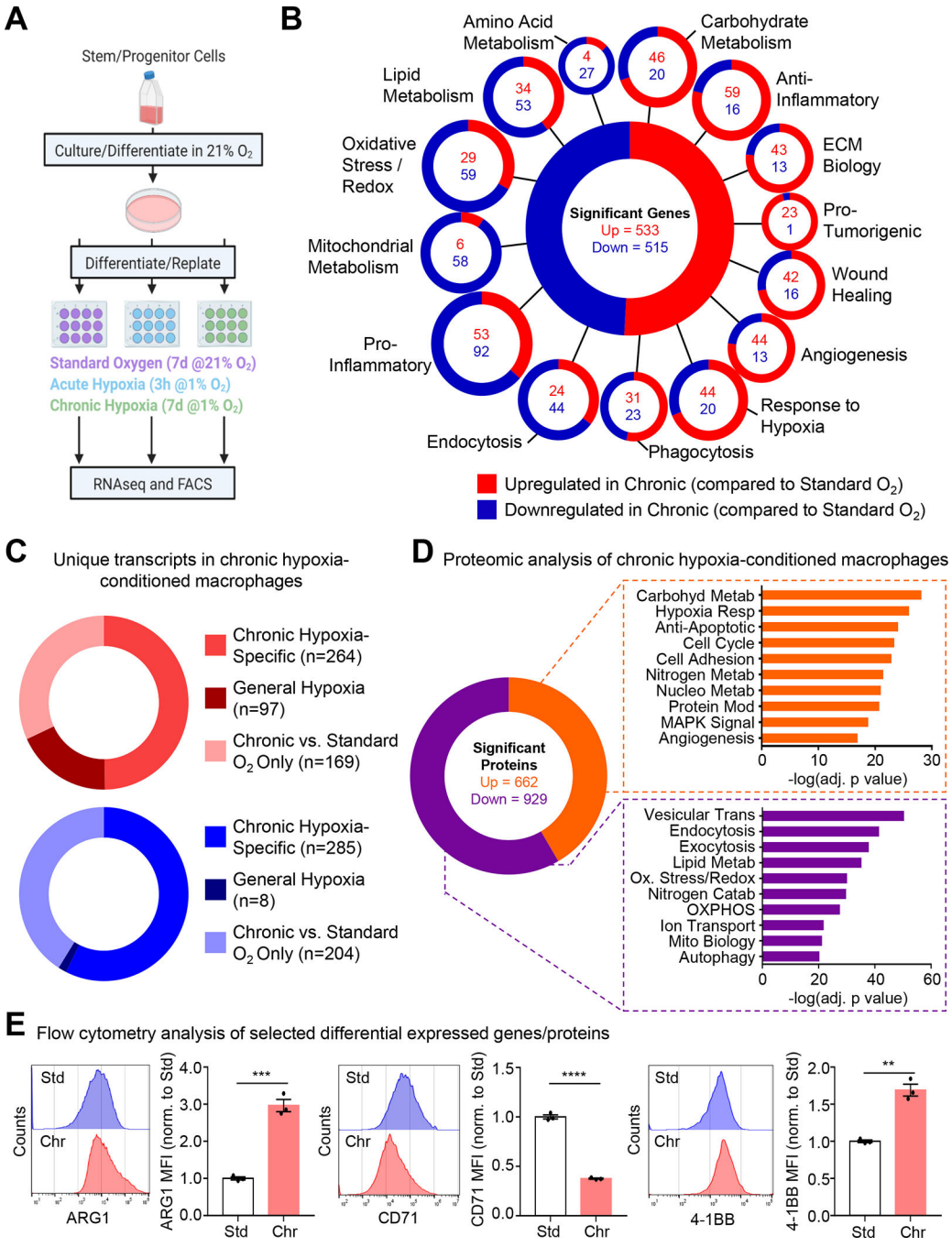

Figure 2: Characterization of macrophages under chronic physiological hypoxia

(A, B) (A) Schematic of method used for RNA sequencing analysis. (B) Shown are classifications of differentially expressed genes according to known or putative function. Three independent experiments were analyzed for each condition. ECM, extracellular matrix.

(C) Analysis of data from (A) to identify unique transcripts in chronic hypoxia-conditioned macrophages compared to standard oxygen and acute hypoxia ('Chronic Hypoxia-Specific'), differentially regulated under acute hypoxia and maintained during

chronic conditioning ('General Hypoxia'), or differentially regulated in chronic hypoxia-conditioned macrophages compared to standard oxygen ('Chronic vs. Standard O_2 Only'). (D) Similar to (A) but instead analyzed via TMT-labeled mass spectrometry. Shown are differentially expressed proteins classified according to known or putative function. Six independent experiments were analyzed for each condition. MAPK, mitogen-activated protein kinase. OXPHOS, oxidative phosphorylation. Pathway significance was determined using Fisher's Exact Tests.

(E) Representative flow cytometry histograms and normalized mean fluorescence intensity (MFI) from analysis of macrophages conditioned as in (A). Data represent three independent experiments, shown as mean ± SEM. Significance was determined by Student's t-test. **p < 0.01. ***p < 0.001. ****p < .0001.

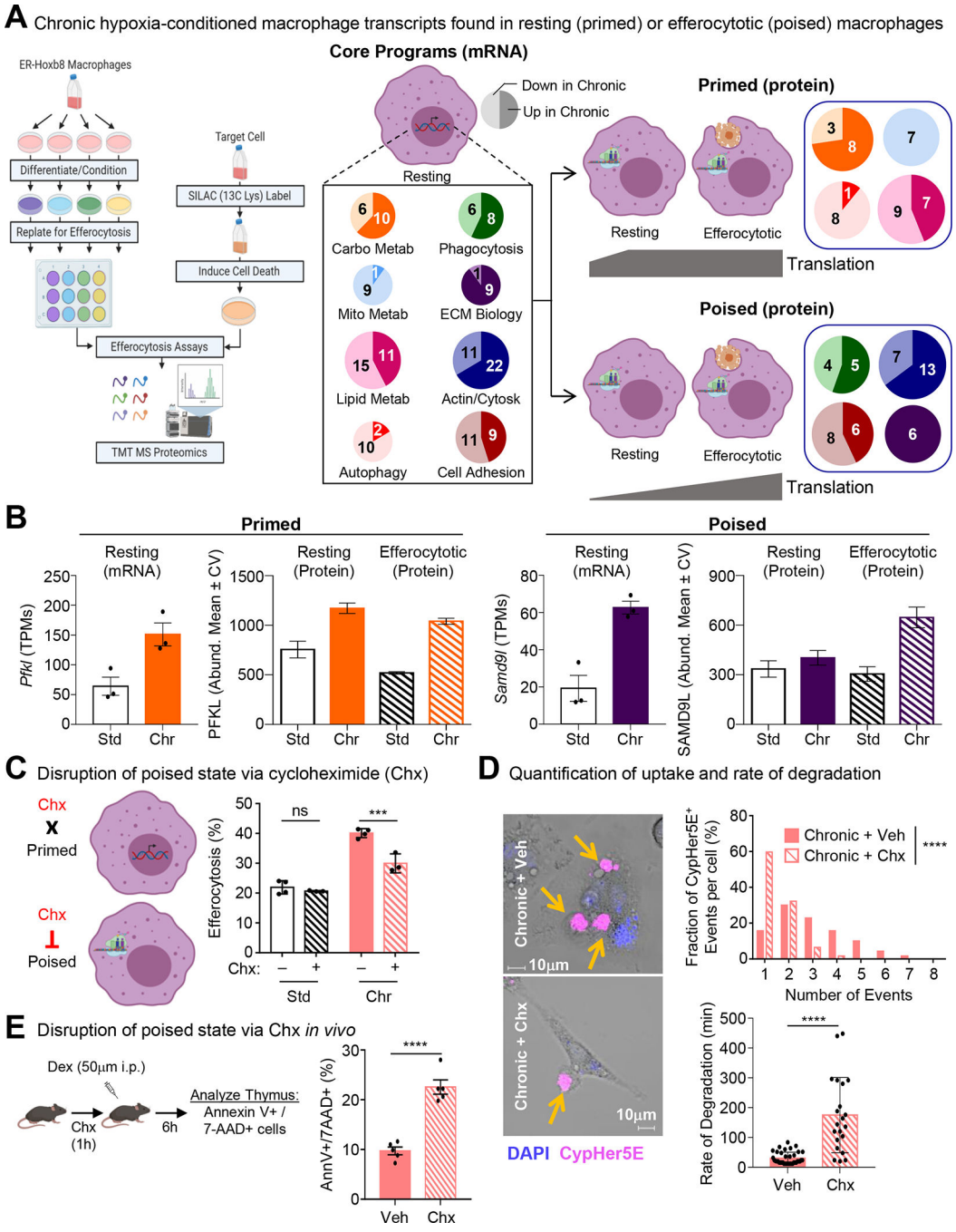

Fig 3: Chronic hypoxia induces states both primed and poised for efferocytosis

(A) Similar to Figure 1A, except macrophages were co-cultured with apoptotic MDA-MB-231s labeled with ^{13}C-Lysine then analyzed via mass spectrometry. Four independent experiments were analyzed for each condition. (Middle/Right) Differentially regulated mRNA transcripts (Core Programs; Middle) were either concomitantly differentially regulated at the protein level in AC-naïve macrophages (Primed; Top Right) or not differentially regulated in AC-naïve macrophages but instead were differentially regulated in efferocytotic macrophages (Poised; Bottom Right). Numbers represent genes/proteins

differentially regulated, with light shading representing downregulated and dark shading representing upregulated.

(B) Shown are representative transcripts/proteins from each state observed in Figure 3A. PFKL/*Pfkl*, ATP-dependent 6-phosphofructokinase, liver-type. SAMD9L/*Samd9l*, Sterile alpha motif domain-containing protein 9-like.

(C) (Left) Schematic illustrating the differential effect of cycloheximide (Chx) treatment on 'primed' versus 'poised' programs. (Right) Experiments performed as in Figure 1A, but with the addition of cycloheximide treatment. Data represent three independent experiments, shown as mean ± SEM.

(D) Experiments performed and analyzed as in Figure 1E. Shown are representative images (Left), quantification of CypHer5E+ events per-cell (Top Right), and analysis of degradation rate (Bottom Right). For quantification, 70 efferocytotic macrophages from 5 vehicle-treated scenes and 62 efferocytotic macrophages from 7 Chx-treated scenes were analyzed. For degradation rate, 38 (vehicle-treated) and 21 (Chx-treated) efferocytotic macrophages were analyzed. Data shown as mean ± SEM.

(E) Schematic of experimental design (Left) and summary plot (Right) of AnnexinV+ 7-AAD+ thymocytes 6h post-dexamethasone (Dex) injection in vehicle (n=5) or cycloheximide (Chx)-treated mice (n=5). Data shown as mean ± SEM.

Significance was determined by Student's t-test in D,E, and by one-way ANOVA in C,D, ***$p < .001$, ****$p < .0001$. ns = not significant.

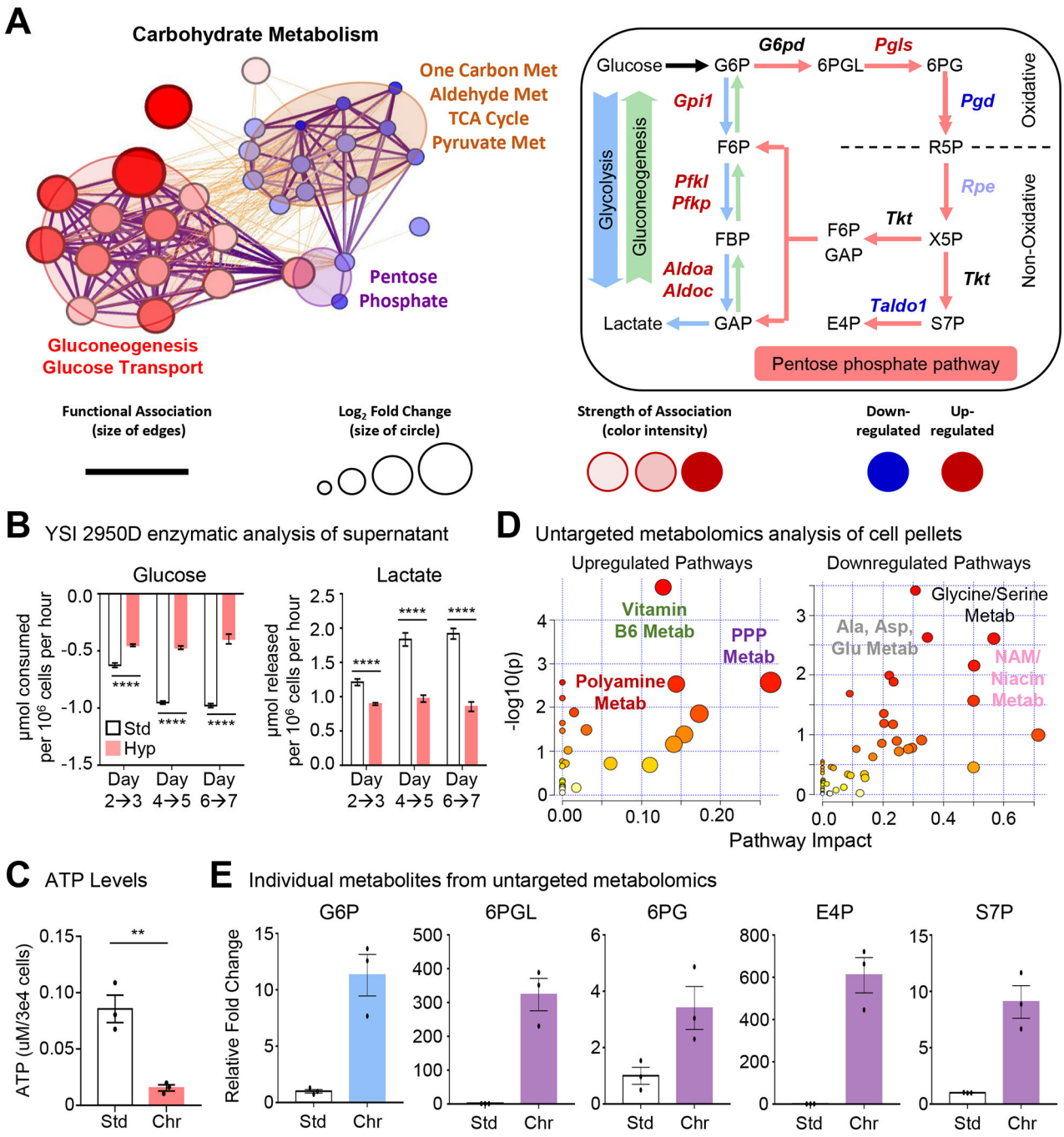

Figure 4: Metabolic pathway use in chronic physiological hypoxia-conditioned macrophages

(A) (Left) Differentially regulated metabolic genes (Figure 2) are represented using network analysis. (Right) Schematic of routes of glucose use. Genes in red are significantly upregulated whereas genes in blue are downregulated.

(B) Macrophages cultured as in Figure 1A but with glucose and lactate media levels in the media analyzed. Data is from two independent experiments, with four biological replicates per experiment. Data are shown as mean ± SEM.

(C) Macrophages cultured as in Figure 1A but analyzed for cellular ATP levels. Data is from three independent experiments, shown as mean ± SEM.

(D) Macrophages cultured as in Figure 1A then isolated for untargeted metabolomic analysis. (Left) upregulated and (Right) downregulated pathways in chronic hypoxia-conditioned macrophages are shown. Three independent experiments were performed for each condition.

(E) Shown are representative metabolites from Figure 4C. Data are shown as mean ± SEM. All metabolites are significant, $p < .0001$. G6P, glucose 6-phosphate. 6PGL, 6-phosphogluconolactone. 6PG, 6-phosphogluconate. E4P, erythrose 4-phosphate. S7P, sedoheptulose 7-phosphate.

Significance was determined by Student's t-test in C, and by one-way ANOVA in B, $**p < .01$, $****p < .0001$.

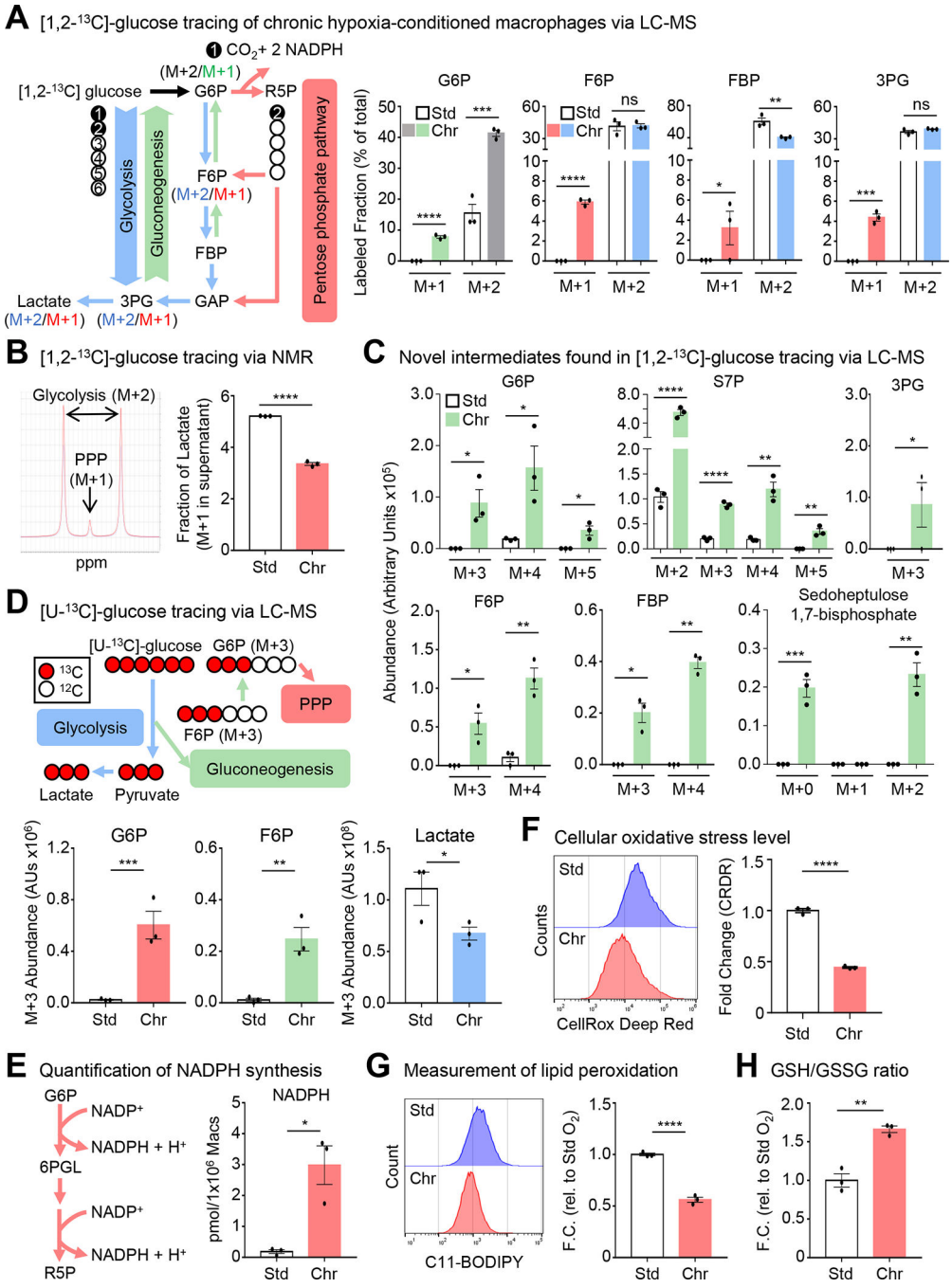

Figure 5: Macrophages co-opt noncanonical pentose phosphate loop for redox homeostasis

(A) (Left) Schematic for isotopologue analysis of [1,2-^{13}C]-glucose tracing experiments. (Right) Macrophages conditioned as in Figure 1A, but cultured with media containing [1,2-^{13}C]-glucose for 16h then analyzed via LC-MS. Shown is the fractional enrichment of the indicated isotopologues. Three independent experiments were performed for each condition. Data are shown as mean ± SEM. G6P, glucose 6-phosphate. F6P, fructose 6-phosphate. FBP, fructose 1,6-bisphosphate. 3PG, 3-phosphoglyceric acid.

(B) (Left) Macrophages conditioned as in Figure 1A. Representative peaks for PPP- and glycolysis-derived lactate in media analyzed via NMR. (Right) Cumulative data of the M+1 lactate fraction. Data are from four biological replicates, shown as mean ± SEM.
(C) Analysis of experiments from Figure 5A. Data shown as mean ± SEM. G6P, glucose 6-phosphate. S7P, sedoheptulose 7-phosphate. 3PG, 3-phosphoglyceric acid. F6P, fructose 6-phosphate. FBP, fructose 1,6-bisphosphate.
(D) (Top) Schematic for [U-^{13}C]-glucose flux analysis. (Bottom) Similar to Figure 5A, except using [U-^{13}C]-glucose. Shown is the relative abundance of the indicated isotopologues. Data are from three independent experiments, shown as mean ± SEM. G6P, glucose 6-phosphate. F6P, fructose 6-phosphate.
(E) (Left) Schematic of NADPH synthesis via PPP. (Right) Macrophages conditioned as in Figure 5A, followed by NADPH quantification. Data are from three independent experiments, shown as mean ± SEM.
(F) Macrophages conditioned as in Figure 5A. Oxidative stress levels were measured using CellRox Deep Red. Shown are representative flow cytometry plots (Left) and summary plots (Right). Data are representative of three independent experiments, shown as mean ± SEM.
(G) Experiments performed as in Figure 5A. Lipid peroxidation was measured using C11-BODIPY 581/591. Shown are representative flow cytometry plots (Left) and summary plots (Right). Data are representative of three independent experiments, shown as mean ± SEM.
(H) Experiments performed as in Figure 5A, then analyzed for total glutathione, reduced glutathione (GSH), and oxidized glutathione (GSSG). Data are from four independent experiments, shown as mean ± SEM.
Significance was determined by Student’s t-test in B,D-H, and by one-way ANOVA in A,C, *p < .05, **p < .01, ***p < .001, ****p < .0001. ns = not significant.

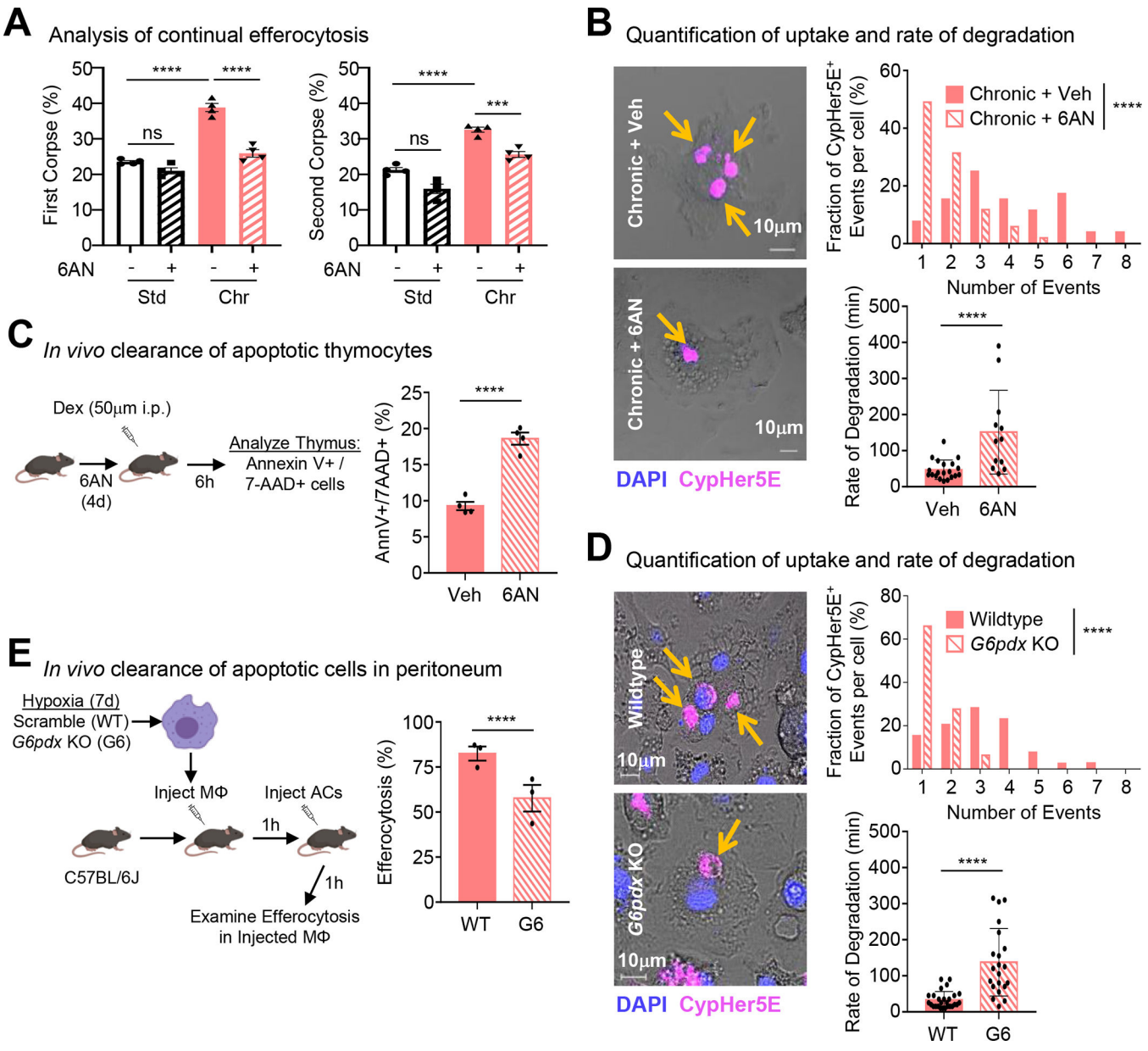

Figure 6: Noncanonical pentose phosphate loop supports continual efferocytosis

(A) Continual efferocytosis experiments performed as in Figure 1D. Data represent three independent experiments, shown as mean ± SEM.

(B) Experiments performed and analyzed as in Figure 1E. Shown are representative images (Left), quantification of CypHer5E+ events per-cell (Top Right), and analysis of degradation rate (Bottom Right). For quantification, 53 efferocytotic macrophages from 5 vehicle-treated scenes and 51 efferocytotic macrophages from 7 6AN-treated scenes were analyzed. For degradation rate, 21 (vehicle-treated) and 13 (6AN-treated) efferocytotic macrophages were analyzed. Data shown as mean ± SEM.

(C) Schematic of experimental design (Left) and summary plot (Right) of AnnexinV+ 7-AAD+ thymocytes 6h post-dexamethasone (Dex) injection in vehicle (n=4) or 6AN-treated mice (n=4). Data shown as mean ± SEM.

(D) Experiments performed and analyzed as in Figure 1E except using G6PDX-deficient (G6) macrophages. Shown are representative images (Left), quantification of CypHer5E+ events (Top Right), and analysis of degradation rate (Bottom Right). For quantification, 39 efferocytotic macrophages from 5 WT scenes and 47 efferocytotic macrophages from 7 G6pdx-deficient scenes were analyzed. For degradation rate, 27 (WT) and 21 (G6pdx-deficient) efferocytotic macrophages were analyzed. Data shown as mean ± SEM.
(E) (Left) Schematic of experimental design. (Right) Summary plot of efferocytosis rate by GFP+ CD11b+ F4/80+ macrophages in WT mice (n=3) and G6pdx-deficient mice (n=3). Data shown as mean ± SEM.
Significance was determined by Student's t-test in B-E, and by one-way ANOVA in A,B,D, ***p < .001, ****p < .0001. ns = not significant.

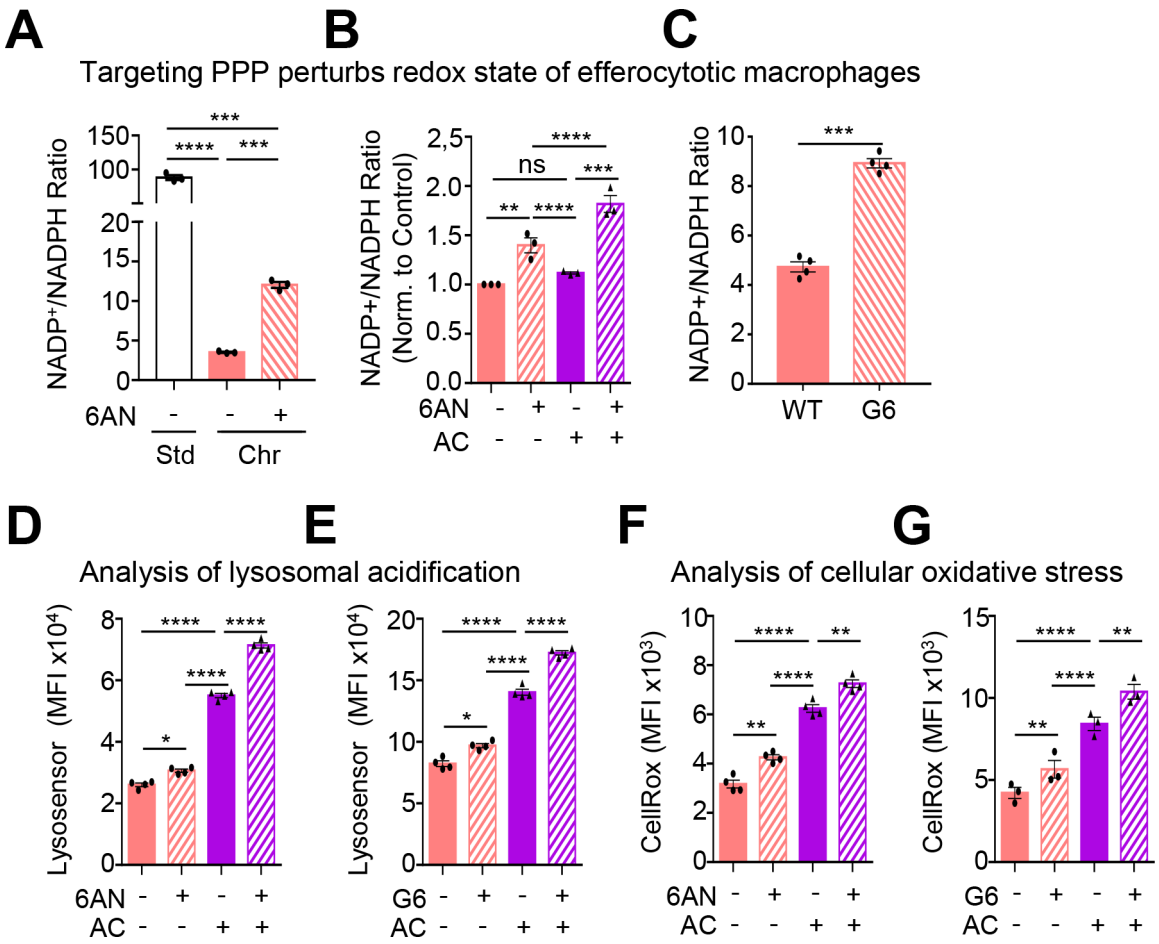

Figure 7: Noncanonical pentose phosphate loop prevents redox crisis in efferocytotic macrophages

(A) Experiments performed as in Figure 1A, with inclusion of 6AN. Data are from three independent experiments, shown as mean ± SEM.

(B) Experiments performed as in Figure 7A. Data are from three independent experiments, shown as mean ± SEM.

(C) Experiments performed as in Figure 7A except using G6PDX-deficient (G6) macrophages. Data are from three independent experiments, shown as mean ± SEM.

(D, E) Experiments performed as in Figure 7A using 6AN-treated macrophages (**D**) or G6PDX-deficient (G6) macrophages (**E**). Lysosomal acidification was measured in efferocytotic macrophages (CypHer5E$^+$). Shown are representative flow cytometry plots (Left) and MFI (Right) from three independent experiments. Data are shown as mean ± SEM.

(F, G) Experiments performed as in Figure 7A using 6AN-treated macrophages (**F**) or G6PDX-deficient (G6) macrophages (**G**). Cellular ROS was measured in efferocytotic macrophages (CypHer5E$^+$). Shown are representative flow cytometry plots (Left) and MFI (Right) from three independent experiments. Data are shown as mean ± SEM.

Significance was determined by Student's t-test in C, and by one-way ANOVA in A,B,D-G, *p < .05, **p < .01, ***p < .001, ****p < .0001. ns = not significant.

Key resources table

REAGENT or RESOURCE	SOURCE	IDENTIFIER
Antibodies		
β-actin	SCBT	sc-47778
G6PDX	Abcam	ab91034
CD16/32 (FcR block)	BioxCell	BP0307
CD11b	eBioscience	48-0112-82
F4/80	eBioscience	12-4801-82
Annexin V	Biolegend	640912
Bacterial and virus strains		
Biological samples		
Thymocytes	C57BL/6J mice	
Bone marrow macrophages	C57BL/6J mice	
Splenic macrophages	C57BL/6J mice	
Chemicals, peptides, and recombinant proteins		
CypHer5E NHS Ester	Cytiva	PA15405
5(6)-TAMRA, SE	ThermoFisher	C1171
Cycloheximide	Sigma	C4859
6-AN	MedChemExpress	HY-W010342
G6PDi-1	Cayman Chemicals	31484
FBP1i	Cayman Chemicals	18860
CFSE	ThermoFisher	C34554
Dexamethasone	Sigma	D4902
7-AAD	Biolegend	420403
13C6-lysine	Cambridge Isotopes	201740-81-0
12C6-arginine	Cambridge Isotopes	1119-34-2
[1,2-13C]-glucose	Cambridge Isotopes	138079-87-5
[U-13C]-glucose	Cambridge Isotopes	110187-42-3
MitoSOX Red	ThermoFisher	M36008
MitoTracker Green	ThermoFisher	M7514
MitoTracker Red	ThermoFisher	M22425
BODIPY 581/591 C11	ThermoFisher	D3861
CellRox Deep Red	ThermoFisher	C10491
Lysosensor Green DND-189	ThermoFisher	L7535
Critical commercial assays		
NADP/NADPH Quantitation Colorimetric Kit	BioVision	K347
GSH/GSSG-Glo Assay	Promega	V6611
Luminescent ATP Detection Assay Kit	Abcam	ab113849

REAGENT or RESOURCE	SOURCE	IDENTIFIER
Deposited data		
mRNA sequencing data	NCBI GEO	GSE192969
Data S1 – Source Data		
Experimental models: Cell lines		
Jurkat T lymphoma	ATCC	TIB-152
MDA-MB-231	MSKCC	
BrM2	MSKCC	
E0771	CH3 Biosystems	94A001
Experimental models: Organisms/strains		
C57BL6/J mice	JAX	000664
Oligonucleotides		
Recombinant DNA		
Mouse G6pdx ORF	OriGene	MR208269
Software and algorithms		
GraphPad Prism 7		
SPSS v.22		
R v.4.0.5		
Gephi v.0.9.1		
Other		

LIFE SCIENCE TABLE WITH EXAMPLES FOR AUTHOR REFERENCE

REAGENT or RESOURCE	SOURCE	IDENTIFIER
Antibodies		
Rabbit monoclonal anti-Snail	Cell Signaling Technology	Cat#3879S; RRID: AB_2255011
Mouse monoclonal anti-Tubulin (clone DM1A)	Sigma-Aldrich	Cat#T9026; RRID: AB_477593
Rabbit polyclonal anti-BMAL1	This paper	N/A
Bacterial and virus strains		
pAAV-hSyn-DIO-hM3D(Gq)-mCherry	Krashes et al.[1]	Addgene AAV5; 44361-AAV5
AAV5-EF1a-DIO-hChR2(H134R)-EYFP	Hope Center Viral Vectors Core	N/A
Cowpox virus Brighton Red	BEI Resources	NR-88
Zika-SMGC-1, GENBANK: KX266255	Isolated from patient (Wang et al.[2])	N/A
Staphylococcus aureus	ATCC	ATCC 29213
Streptococcus pyogenes: M1 serotype strain: strain SF370; M1 GAS	ATCC	ATCC 700294
Biological samples		
Healthy adult BA9 brain tissue	University of Maryland Brain & Tissue Bank; http://medschool.umaryland.edu/btbank/	Cat#UMB1455
Human hippocampal brain blocks	New York Brain Bank	http://nybb.hs.columbia.edu/
Patient-derived xenografts (PDX)	Children's Oncology Group Cell Culture and Xenograft Repository	http://cogcell.org/
Chemicals, peptides, and recombinant proteins		
MK-2206 AKT inhibitor	Selleck Chemicals	S1078; CAS: 1032350-13-2
SB-505124	Sigma-Aldrich	S4696; CAS: 694433-59-5 (free base)
Picrotoxin	Sigma-Aldrich	P1675; CAS: 124-87-8
Human TGF-β	R&D	240-B; GenPept: P01137
Activated S6K1	Millipore	Cat#14-486
GST-BMAL1	Novus	Cat#H00000406-P01
Critical commercial assays		
EasyTag EXPRESS 35S Protein Labeling Kit	PerkinElmer	NEG772014MC
CaspaseGlo 3/7	Promega	G8090
TruSeq ChIP Sample Prep Kit	Illumina	IP-202-1012
Deposited data		
Raw and analyzed data	This paper	GEO: GSE63473
B-RAF RBD (apo) structure	This paper	PDB: 5J17

REAGENT or RESOURCE	SOURCE	IDENTIFIER
Human reference genome NCBI build 37, GRCh37	Genome Reference Consortium	http://www.ncbi.nlm.nih.gov/projects/genome/assembly/grc/human/
Nanog STILT inference	This paper; Mendeley Data	http://dx.doi.org/10.17632/wx6s4mj7s8.2
Affinity-based mass spectrometry performed with 57 genes	This paper; Mendeley Data	Table S8; http://dx.doi.org/10.17632/5hvpvspw82.1
Experimental models: Cell lines		
Hamster: CHO cells	ATCC	CRL-11268
D. melanogaster: Cell line S2: S2-DRSC	Laboratory of Norbert Perrimon	FlyBase: FBtc0000181
Human: Passage 40 H9 ES cells	MSKCC stem cell core facility	N/A
Human: HUES 8 hESC line (NIH approval number NIHhESC-09-0021)	HSCI iPS Core	hES Cell Line: HUES-8
Experimental models: Organisms/strains		
C. elegans: Strain BC4011: srl-1(s2500) II; dpy-18(e364) III; unc-46(e177)rol-3(s1040) V.	Caenorhabditis Genetics Center	WB Strain: BC4011; WormBase: WBVar00241916
D. melanogaster: RNAi of Sxl. y[1] sc[*] v[1]; P{TRiP.HMS00609}attP2	Bloomington Drosophila Stock Center	BDSC:34393; FlyBase: FBtp0064874
S. cerevisiae: Strain background: W303	ATCC	ATTC: 208353
Mouse: R6/2: B6CBA-Tg(HDexon1)62Gpb/3J	The Jackson Laboratory	JAX: 006494
Mouse: OXTRfl/fl: B6.129(SJL)-Oxtr$^{tm1.1Wsy}$/J	The Jackson Laboratory	RRID: IMSR_JAX:008471
Zebrafish: Tg(Shha:GFP)t10: t10Tg	Neumann and Nuesslein-Volhard[3]	ZFIN: ZDB-GENO-060207-1
Arabidopsis: 35S::PIF4-YFP, BZR1-CFP	Wang et al.[4]	N/A
Arabidopsis: JYB1021.2: pS24(AT5G58010)::cS24:GFP(-G):NOS #1	NASC	NASC ID: N70450
Oligonucleotides		
siRNA targeting sequence: PIP5K I alpha #1: ACACAGUACUCAGUUGAUA	This paper	N/A
Primers for XX, see Table SX	This paper	N/A
Primer: GFP/YFP/CFP Forward: GCACGACTTCTTCAAGTCCGCCATGCC	This paper	N/A
Morpholino: MO-pax2a GGTCTGCTTTGCAGTGAATATCCAT	Gene Tools	ZFIN: ZDB-MRPHLNO-061106-5
ACTB (hs01060665_g1)	Life Technologies	Cat#4331182
RNA sequence: hnRNPA1_ligand: UAGGGACUUAGGGUUCUCUCUAGGGACUUAGGGUUCUCUCUAGGGA	This paper	N/A
Recombinant DNA		
pLVX-Tight-Puro (TetOn)	Clonetech	Cat#632162
Plasmid: GFP-Nito	This paper	N/A
cDNA GH111110	Drosophila Genomics Resource Center	DGRC:5666; FlyBase:FBcl0130415
AAV2/1-hsyn-GCaMP6- WPRE	Chen et al.[5]	N/A
Mouse raptor: pLKO mouse shRNA 1 raptor	Thoreen et al.[6]	Addgene Plasmid #21339

REAGENT or RESOURCE	SOURCE	IDENTIFIER
Software and algorithms		
ImageJ	Schneider et al.[7]	https://imagej.nih.gov/ij/
Bowtie2	Langmead and Salzberg[8]	http://bowtie-bio.sourceforge.net/bowtie2/index.shtml
Samtools	Li et al.[9]	http://samtools.sourceforge.net/
Weighted Maximal Information Component Analysis v0.9	Rau et al.[10]	https://github.com/ChristophRau/wMICA
ICS algorithm	This paper; Mendeley Data	http://dx.doi.org/10.17632/5hvpvspw82.1
Other		
Sequence data, analyses, and resources related to the ultra-deep sequencing of the AML31 tumor, relapse, and matched normal	This paper	http://aml31.genome.wustl.edu
Resource website for the AML31 publication	This paper	https://github.com/chrisamiller/aml31SuppSite

PHYSICAL SCIENCE TABLE WITH EXAMPLES FOR AUTHOR REFERENCE

REAGENT or RESOURCE	SOURCE	IDENTIFIER
Chemicals, peptides, and recombinant proteins		
QD605 streptavidin conjugated quantum dot	Thermo Fisher Scientific	Cat#Q10101MP
Platinum black	Sigma-Aldrich	Cat#205915
Sodium formate BioUltra, ≥99.0% (NT)	Sigma-Aldrich	Cat#71359
Chloramphenicol	Sigma-Aldrich	Cat#C0378
Carbon dioxide (^{13}C, 99%) (<2% ^{18}O)	Cambridge Isotope Laboratories	CLM-185-5
Poly(vinylidene fluoride-co-hexafluoropropylene)	Sigma-Aldrich	427179
PTFE Hydrophilic Membrane Filters, 0.22 μm, 90 mm	Scientificfilters.com/Tisch Scientific	SF13842
Critical commercial assays		
Folic Acid (FA) ELISA kit	Alpha Diagnostic International	Cat# 0365-0B9
TMT10plex Isobaric Label Reagent Set	Thermo Fisher	A37725
Surface Plasmon Resonance CM5 kit	GE Healthcare	Cat#29104988
NanoBRET Target Engagement K-5 kit	Promega	Cat#N2500
Deposited data		
B-RAF RBD (apo) structure	This paper	PDB: 5J17
Structure of compound 5	This paper; Cambridge Crystallographic Data Center	CCDC: 2016466
Code for constraints-based modeling and analysis of autotrophic *E. coli*	This paper	https://gitlab.com/elad.noor/sloppy/tree/master/rubisco
Software and algorithms		
Gaussian09	Frish et al.[1]	https://gaussian.com
Python version 2.7	Python Software Foundation	https://www.python.org
ChemDraw Professional 18.0	PerkinElmer	https://www.perkinelmer.com/category/chemdraw
Weighted Maximal Information Component Analysis v0.9	Rau et al.[2]	https://github.com/ChristophRau/wMICA
Other		
DASGIP MX4/4 Gas Mixing Module for 4 Vessels with a Mass Flow Controller	Eppendorf	Cat#76DGMX44
Agilent 1200 series HPLC	Agilent Technologies	https://www.agilent.com/en/products/liquid-chromatography
PHI Quantera II XPS	ULVAC-PHI, Inc.	https://www.ulvac-phi.com/en/products/xps/phi-quantera-ii/